Article

Current Biology

Non-uniform signal pooling across the foveola

Highlights

- We measured foveal crowding using retinally stabilized stimuli
- Critical spacing at the PRL matched the diameter of a single cone
- Crowding exceeded cone spacing and caused mislocalization 0.25° from PRL
- Results reveal increasing signal pooling across the foveola

Authors

Krishnamachari S. Prahalad, Ashley M. Clark, Benjamin Moon, ..., Michele Rucci, Jannick P. Rolland, Martina Poletti

Correspondence

pkrishn5@ur.rochester.edu

In brief

Prahalad et al. use high-resolution retinal imaging with retinal-contingent stimulus delivery to show that within the foveola, crowding at the preferred retinal locus matches cone spacing but exceeds it just 0.25° away, where mislocalization emerges, indicating increased signal pooling with foveolar eccentricity.

Prahalad et al., 2025, Current Biology *35*, 6086–6099
December 15, 2025
https://doi.org/10.1016/j.cub.2025.11.007

CellPress

CellPress

Current Biology

Article

Non-uniform signal pooling across the foveola

Krishnamachari S. Prahalad,[1,2,8,*] Ashley M. Clark,[1,2] Benjamin Moon,[2,3] Austin Roorda,[6] Pavan Tiruveedhula,[6] Wolf Harmening,[7] Aleksandr Gutnikov,[7] Samantha K. Jenks,[1,2] Sanjana Kapisthalam,[1,2] Michele Rucci,[1,2,4] Jannick P. Rolland,[2,3,5] and Martina Poletti[1,2,4]

[1]Department of Brain and Cognitive Sciences, University of Rochester, Meliora Hall, Rochester, NY 14627, USA
[2]Center for Visual Science, University of Rochester, 361 Meliora Hall, Rochester, NY 14627, USA
[3]Institute of Optics, University of Rochester, Rochester, NY 14627, USA
[4]Department of Neuroscience, University of Rochester, 601 Elmwood Avenue, Rochester, NY 14642, USA
[5]Department of Biomedical Engineering, University of Rochester, Goergen Hall, Rochester, NY 14627, USA
[6]Herbert Wertheim School of Optometry and Vision Science, University of California, Berkeley, 581 Minor Hall, Berkeley, CA 94720, USA
[7]Department of Ophthalmology, Rheinische Friedrich-Wilhelms-Universität Bonn, Sigmund-Freud-Str. 25, 53127 Bonn, Germany
[8]Lead contact
*Correspondence: pkrishn5@ur.rochester.edu
https://doi.org/10.1016/j.cub.2025.11.007

SUMMARY

Object recognition is impacted by visual crowding. This phenomenon, attributed to cortical pooling, is generally studied in the periphery. Crowding mechanisms in the foveola—the 1° retinal region with highest resolution—remain unclear due to difficulties in controlling for optical factors and incessant fixational eye motion. Using high-resolution retinal imaging and retinal-contingent stimulus rendering to overcome these limitations, we demonstrated that the critical spacing at the preferred retinal locus approximates a single cone's diameter. However, just 0.25° away, mislocalization errors start to occur and the extent of crowding exceeds cone spacing. These results reveal that cortical pooling mechanisms may play a greater role with increasing foveolar eccentricity and point to a possible cortical magnification gradient effect within the central fovea.

INTRODUCTION

Objects are rarely encountered in isolation, instead, they are usually embedded in or cluttered among other objects. In certain circumstances, when the surrounding objects (flankers) get closer to the one of interest, they begin negatively impacting the recognition of that object, even if there is no physical overlap. This phenomenon is referred to as visual crowding.[1–3] The strength of crowding depends on the distance between the target and the surrounding flankers: if the flankers are placed far enough from the target, they no longer affect the recognition of the target. The smallest distance between the target and flanker at which performance drops by a given amount from the asymptotic performance level is referred to as critical spacing. This distance determines the spatial extent of crowding, also known as the "crowding zone." The size of the crowding zone has been shown to change linearly with the eccentricity of the target from the center of gaze,[1] a relationship known as the "Bouma's law." Crowding has been extensively studied in the peripheral visual field, where it is thought to have a stronger impact on object recognition.[3–5] However, much less is known on crowding at the foveal scale. For a long time, it has been debated whether foveal crowding exists. Few studies reported weak or absent crowding effects in the fovea,[6–8] while other studies suggested that its effects extends into the fovea when tested under normal viewing conditions.[9–15] A recent study demonstrated that foveal crowding is not driven by optical limitations.[16] The phenomenon persisted even when stimuli were presented at the eye's diffraction-limited resolution using an adaptive optics scanning light ophthalmoscope (AOSLO), effectively correcting for optical aberrations. Because the foveola supports the highest visual acuity, the existence of crowding in this region is particularly significant and must be carefully analyzed, as it can substantially degrade fine spatial vision. Thus, foveal crowding can impact fine spatial vision in a number of instances when flankers are sufficiently close to the target.

Although it is now accepted that crowding also occurs in the fovea, many open questions remain. First, the relationship between critical spacing and the underlying cone mosaic remains unclear. Understanding the extent of crowding in terms of cone spacing may offer an anatomical reference for the spatial extent of integration, but it is not yet known whether cone spacing directly constrains crowding. This is particularly relevant in the foveola where there is no pooling of the photoreceptor signal at the level of the retinal ganglion cells (RGCs), which, extrafoveally, has an impact on the extent of the cortical pooling regions.[17–20] Second, if and how the extent of crowding changes with small increments of eccentricity from the center of gaze within the 1° foveolar region, where visual functions are often assumed to be uniform. Third, whether and how the location of surrounding stimuli (inner vs. outer) differentially modulates crowding as we move away from the preferred retinal locus of fixation (PRL). This is the retinal location preferentially used to center stimuli on during fixation, which is distinct from the pseudo-fovea described in low vision; the latter emerging as a compensatory strategy when the anatomical fovea is no longer

functional.[21,22] Fourth, by examining the pattern of photoreceptors stimulated by the target and the surrounding distractors during fixation, this study can provide additional insights into the influence of fixational eye movements (FEMs) on foveal crowding, previously observed in the presence of the habitual optical imperfections of the eye.[14] In normal viewing conditions optical aberrations can blur the stimuli, potentially activating more cones, while FEMs can move the stimuli across multiple receptors and pooling regions, influencing the estimates of critical spacing. Therefore, correcting for optical aberrations and retinally stabilizing the stimuli by fixing them on a retinal landmark in real time become important to ensure that the observed crowding effects are not influenced by these confounds. This approach makes it possible to unambiguously determine which cones are stimulated by the target and which fall between the target and the flankers to directly assess the relationship between critical spacing and cone spacing. Notably, previous studies have not simultaneously controlled for optical and oculomotor factors in this way, leaving this issue open. Addressing it is important to shed light on the mechanisms underlying visual processing and segmentation across the central fovea.

It is well known that foveal and peripheral vision differ fundamentally in photoreceptor distribution and visual pathway wiring.[23] RGCs, which transmit visual information to the cortex,[24] are distributed non-uniformly across the retina,[25–27] and this uneven distribution gives rise to cortical magnification, whereby a disproportionately large portion of V1 is dedicated to foveal input.[28–30] The 1° foveola is anatomically distinct from the rest of the retina, as it has dense cone packing and no vasculature, supporting fine spatial detail.[23,31] Each cone connects to dedicated ON and OFF bipolar cells projecting to distinct midget RGCs,[17–20] enabling high-resolution transmission. In the central fovea, when optical aberrations are corrected, visual acuity matches cone spacing estimates, indicating that cone spacing—not RGC convergence—sets acuity limits.[32] Just outside the fovea, and even at the edge of the foveola,[32] multiple photoreceptors converge onto single RGCs,[23,31] and this convergence together with RGC density sets acuity limits in this region.[32] Notably, visual acuity and crowding are not equivalent; while acuity refers to the spatial resolving capacity of the visual system, i.e., the ability to discriminate fine details or distinguish two points as separate, crowding reflects impaired stimulus recognition due to interference from nearby objects. Beyond limiting resolution, RGC convergence has been linked to crowding.[33,34] Yet, crowding is also shaped by higher-level mechanisms, including cortical[35–37] and attentional factors.[38,39] Dichoptic studies further show that crowding persists when target and flankers are presented to different eyes.[40,41] According to pooling accounts, crowding reflects excessive integration of target and flanker signals within the crowding zone, with further pooling thought to begin in V1 and increase along the visual pathway.[5,42–47] Importantly, crowding is not obligatory: spatial arrangements that promote grouping/segmentation (e.g., collinear flankers and global structure) or feature differences in contrast, color, or depth can reduce or eliminate it.[48–53] Although crowding is well-characterized extrafoveally, it is still unclear how it is modulated with eccentricity across the 1° central fovea. In particular, it remains an open question to what extent photoreceptor spacing and RGC density contributes to foveal crowding. Understanding this relationship would provide valuable insights into how spatial information is integrated in the foveola, and whether crowding at this scale differs from extrafoveal crowding.

In the peripheral visual field, critical spacing follows Bouma's law, but it remains unclear whether this relationship extends into the foveolar region of the fovea (<30′ eccentricity) for stimuli presented at much smaller distances from the PRL. Although cone density has been shown to vary within the foveola,[23,31,54] visual functions such as detection thresholds have been found to be relatively uniform.[55] However, the ability to discriminate fine detail drops as little as 15′ away from the preferred locus of fixation,[56,57] and in a more complex visual context in the presence of microsaccades, contrast detection thresholds have been shown to increase with larger eccentricities in the foveola.[57] It is unknown whether the magnitude of crowding changes with small shifts in stimulus eccentricity within the foveola, or if it is generally uniform throughout this region. The relationship between critical spacing and cortical magnification is closely linked to how visual information is represented in the brain. As a result of cortical magnification, a target and flanker with a fixed distance in the visual field shift closer together cortically with increasing eccentricity. The observed increase in critical spacing with eccentricity has been attributed to this reduction in cortical distance, reflecting how information is organized in the brain.[34,58,59] While cortical magnification and pooling regions involved in crowding have been studied at relatively larger eccentricities from the PRL,[34,58] it remains unclear how it may affect crowing in the foveola. Addressing these issues will provide important insights into signal pooling across this region.

In typical studies examining the critical spacing of visual crowding in the peripheral visual field, FEMs likely do not have an impact on crowding as the spatial extent of crowding is much larger than the magnitude of the FEMs. Yet, the eyes are constantly in motion even as we attempt to fixate. A growing body of evidence has demonstrated that the temporal modulations introduced by ocular drift enhance fine spatial vision and acuity.[56,60–66] These tiny eye movements likely have minimal impact on peripheral crowding—due to the small amplitude of the retinal shift they introduce compared with the size of crowding pooling regions. However, at the foveal level, ocular drifts continuously shift the retinal image of stimuli across many photoreceptors,[14,63,67,68] likely spanning multiple pooling regions over time and thereby exacerbating crowding.[14] Here, to better understand the relationship between cortical and retinal factors in determining the critical spacing, we compared crowding estimates when stimuli were either fixed in space or shifted on the display to compensate for fixational eye movement, a technique known as retinal stabilization.

Probing the mechanisms of foveal crowding is challenging due to the presence of incessant FEMs, which move flankers and targets across the same pooling region over time,[14] and the presence of higher-order optical aberrations that are inherent to the visual system. These aberrations reduce acuity[69,70] and make it difficult to determine the actual crowding extent, as these factors influence crowding at the foveal scale. Addressing this issue is important to further our understanding of how the central foveal input is processed, and for clarifying how information pooling mechanisms that underlie object segmentation and

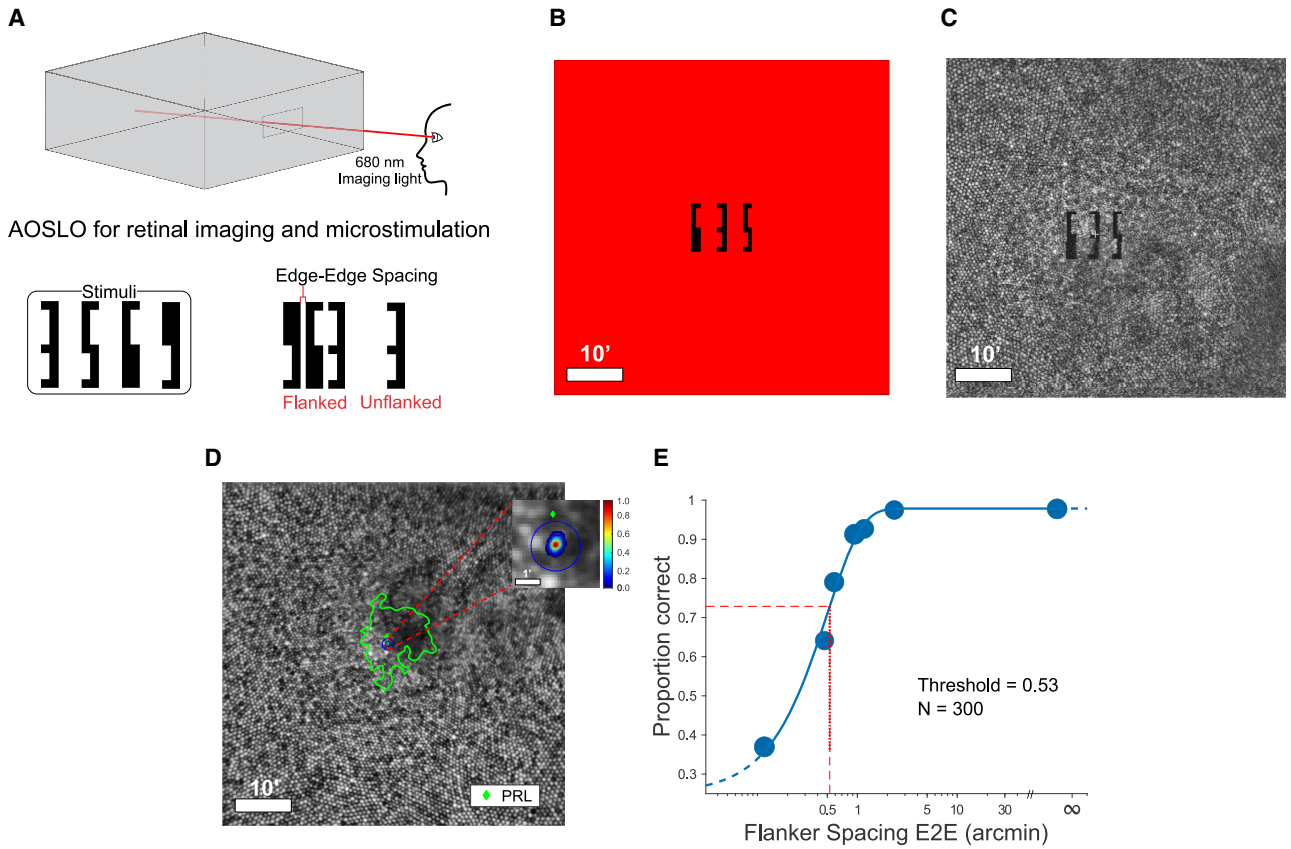

Figure 1. Experimental protocol

(A) Retinal imaging and stimulus delivery was achieved using a custom adaptive optics scanning light ophthalmoscopy (AOSLO). Imaging and stimulus delivery (decrement) was achieved using a 680-nm light, which appeared as a bright red/orange color to observers. Stimuli consisted of digits 3, 5, 6, and 9, rendered using the Pelli font.[9] The target-flanker spacing is represented as the edge-to-edge separation between the two digits.

(B) An example stimulus consisting of target and flankers as it appears to the subject. Stimuli were presented with negative contrast for 500 ms and were delivered to the subject's retina via a 680-nm channel by modulating the laser during raster scanning.

(C) A single frame from a trial with the stimulus rendered at the preferred retinal locus of fixation (PRL) of subject S1, determined before the main experiment. The video frame has been flipped vertically to align with the observer's perspective as shown in B.

(D) The stimulus distribution maps, shown as topographic maps, are overlaid on the retinal image for an example subject. The median PRL location is marked by a green diamond, with the 68% contour highlighted by the green trace. The blue circle highlights the position accuracy threshold used in the current study; only trials with stimuli landing within 1′ from the average of stimulus locations were used. Note that the distribution represents only the locations stimulated by the stimulus center.

(E) An example psychometric fit from subject S1, where performance is plotted against target-flanker spacing represented as the edge-to-edge separation in arcminutes. The blue circles and numbers indicate the tested target-flanker spacings and the number of trials at each spacing.

See also Figures S1 and S2.

recognition are modulated across the foveola. To overcome these challenges and investigate the relationship between cone spacing and the critical spacing of visual crowding across the foveola, we presented stimuli under diffraction-limited conditions,[71–73] and restricted retinal stimulation to targeted eccentricities by controlling for FEMs in real time using retinally contingent stimulus delivery and high-precision eye-tracking.[74,75] Our results show that, at the PRL, critical spacing is roughly the size of a single cone, suggesting that the visual system integrates information from the cones stimulated by the object and the nearest neighboring cone. However, just 15′ away, the critical spacing exceeds cone spacing, indicating increased cortical pooling with eccentricity, even within the foveola. Further, at the PRL, incorrect responses showed no bias in reporting either flanker, but 15′ away, subjects were more likely to report the inner flanker on incorrect trials, suggesting the presence of different mechanisms mediating crowding at this eccentricity. Finally, when stimuli were presented without retinal stabilization, critical spacing increased confirming that fixational instability may exacerbate the effects of crowding.

RESULTS

To examine visual crowding within the foveola, we used digits in Pelli font,[9] a tall and thin font designed specifically to study crowding in the fovea. An AOSLO[71] (see Figure 1A) was used to image at high resolution the foveal cone mosaic, correct for the eye's optical aberrations when rendering stimuli on the

retina, and deliver stimuli to targeted retinal locations using retinal stabilization.[74,75] and extract FEMs from the motion of the foveal cone mosaic over different frames.[76,77] The stimuli appeared either in isolation or were flanked by two other digits along the horizontal axis (Figure 1B). Observers were required to report the central digit. An example frame with the stimulus rendered at the PRL is shown in Figure 1C. The PRL was assessed before the main experiment following the same methodology as previously described[78] (see STAR Methods for details). To ensure that the stimulus size did not limit performance in the crowded recognition task, i.e., it was above the acuity limit, a QUEST procedure (a Bayesian adaptive algorithm for estimating thresholds) was first used to determine the threshold size for an isolated stimulus. Stimulus size was then scaled by a factor of three when presented in the crowded condition, a procedure used before in the literature.[3,79] Stimuli spacings used in the study were as small as ~0.12′; hence, to rule out the possibility that tiny amounts of residual diffraction, after the AOSLO correction, may have influenced our results, we simulated the effects of this residual diffraction by convolving the point spread function in the diffraction-limited condition, based on our subjects' pupil sizes in the experiment, with the crowded stimulus at the closest spacing. Our examination confirms that, even if in this condition (smallest spacing tested, ~0.12′ arcmin) there was a slight blur of the stimuli, there was no physical overlap between stimuli in the retinal image and the boundaries of the stimuli were still clearly visible. This rules out potential confounds related to optical overlap due to diffraction (see Figure S1).

Experiment 1: Critical spacing at the preferred retinal locus of fixation

As ocular drift moves stimuli over multiple receptors and has been shown to impact both acuity and crowding,[14,60,61,65,80] it is crucial to account for fixational eye motion when examining the relationship between cone spacing at the foveal level and the critical spacing. To this end, the crowded stimulus was stabilized at each individual's PRL (see Figure 1D). Performance was found to decrease by 50% ± 9% (two-tailed paired t test, $t(7) = -14.99$, $p < 0.001$, $BF_{10} > 1{,}000$, Cohen's d = 6.17) for the closest flankers spacing that was tested (~0.12′) when compared with the isolated or unflanked stimulus condition (Figure 2A). A similar but less pronounced decrease in performance was observed for the second smallest spacing tested (0.35′ ± 0.12′). Performance for the isolated stimuli (average stimulus width in the crowding condition was 1.85′ ± 0.25′) was near ceiling levels (0.99 ± 0.01), indicating that the size of the stimulus did not limit performance. Instead, performance changes were primarily driven by the separation between the target and the flanker.

Using a similar approach as previous work,[16,79,81,82] we determined the critical spacing, as the edge-to-edge (E2E) distance between the target and flanker yielding a performance drop of 25% from the asymptotic performance level (see STAR Methods for details) (Figure 1E). Since the asymptotic performance levels were close to ceiling for most subjects (~95%), the threshold performance level was found to near 75%. Results show that performance decreased as the target-flanker spacing was reduced, with critical spacing thresholds ranging from 0.20′ to 0.88′ (see Figure S2 for individual psychometric functions).

To understand the relationship between critical spacing and cone spacing, we determined the average cone diameter for the subset of cones falling within the region encompassed by the stimulus array, as shown in the example in Figure 2B. Similarly, Figure 2C highlights the activated cone locations on the Voronoi grid of the underlying cone mosaic for a single frame of stimulus presentation. The E2E flanker spacings were then expressed as multiples of the average cone diameter, which in the foveola approximates center-to-center cone spacing, in the stimulated region (Figure 2D). Our results show that critical spacings ranged between 0.40 to 1.88 times the average cone diameter (0.53′ ± 0.23′). Acuity thresholds across individuals, as determined by the QUEST procedure, were found to be 0.61′ ± 0.20′ and 1.14 ± 0.35 times the cone diameter. The average critical spacings were found to be in the same range; 0.59′ ± 0.22′ and 1.15 ± 0.48 times the cone diameter.

To further investigate the relationship between foveal crowding and cone spacing, we determined the performance levels at flanker spacing levels that corresponded to 0.5×, 1×, and 2× the cone diameter (see STAR Methods for detail). Figure 2E shows the average and individual performance levels at different target-flanker spacings when represented as multiples of cone diameter. When the spacing between stimuli encompassed 1 cone diameter performance was found to be 72% ± 15% across subjects. Performance levels at 0.5× and 2× cone diameter were found to be 58% ± 14% and 83% ± 11%, respectively. Thus, the critical spacing estimates based on a drop of 25% from asymptotic performance level were found to closely match the average cone diameter within the stimulated region, and although performance was still very high, a drop in the average percent of correct responses was already visible for spacings approximately matching 2 cones.

Experiment 2: Influence of foveolar eccentricity on crowding extent

Cone density within the foveola is non-uniform and starts declining at distances that are a few arcminutes away from the peak cone density (PCD).[23,55,83] To test whether such structural changes influence crowding, we asked subjects to perform the same task as in experiment 1, but this time, the stimuli were stabilized ~15′ temporal to the PRL in the visual field, which corresponds to a nasal retinal location in the right eye. Figure 3A illustrates the stimulus distribution map overlaid on the retina marked alongside the PRL (green diamond) for an example subject. Figures 3B and 3C highlight the offset of the stimulus from individual PRL locations and the mean 68% contour area around their respective PRL distributions. Note that the offset from the PRL was much smaller for S3 than the desired target eccentricity (7.24′), resulting in minimal changes in critical spacings between stimuli stabilized at the PRL and the tested eccentricity. This offset was due to inaccuracies in the online registration process, which marks a different retinal coordinate as the target location instead of the intended eccentricity from the PRL. Thus, we excluded this subject's data from subsequent analysis. In addition, we quantified the change in cone density and spacing between the PRL and 15′ eccentricity (Figures 3D and 3E). Cone density was higher at the PRL compared with 15′ (two-tailed paired t test, $t(5) = -9.32$, $p < 0.001$, $BF_{10} = 121.30$, Cohen's d = 1.15), while cone spacing was significantly larger at 15′

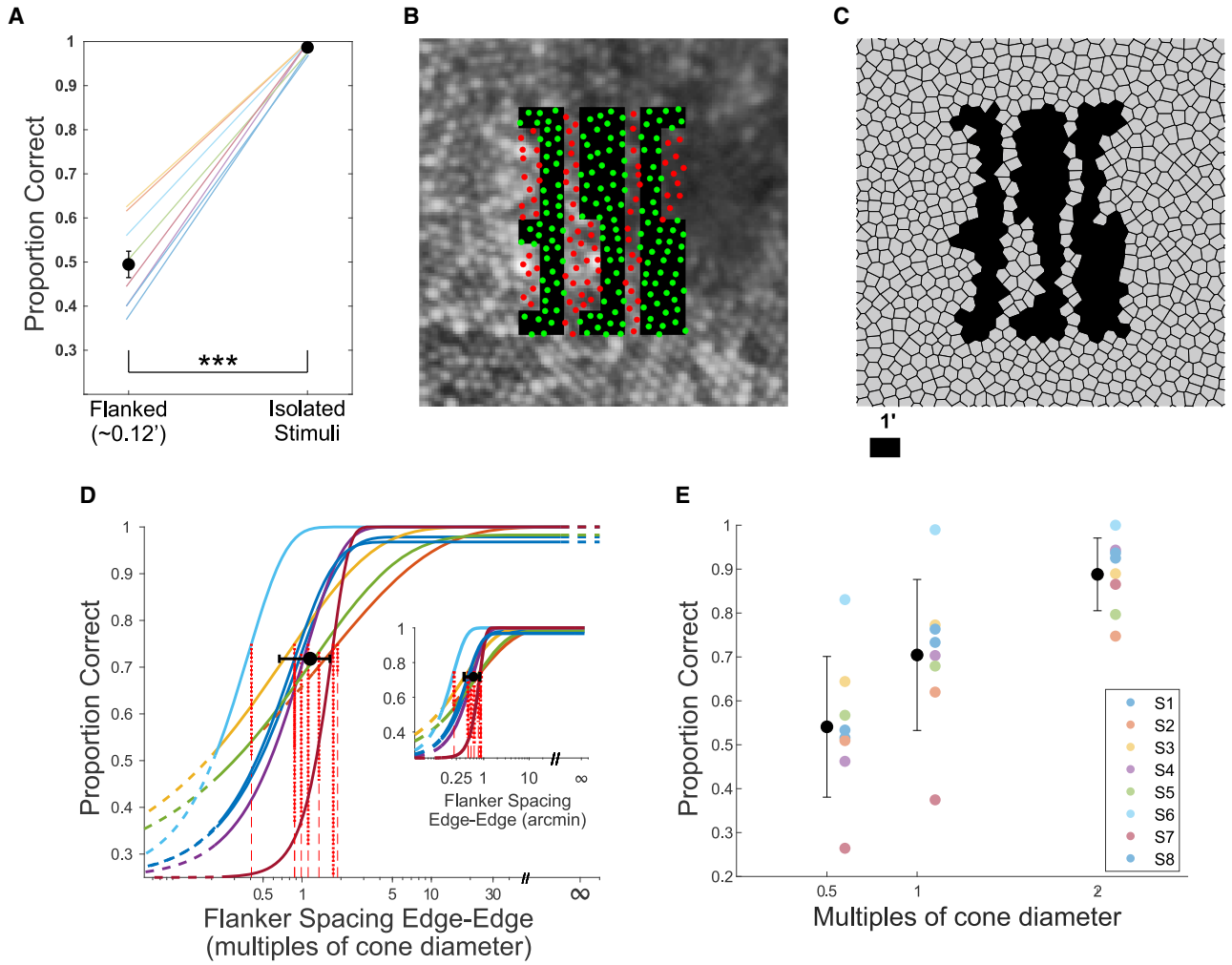

Figure 2. Critical spacing of visual crowding at the PRL

(A) Average performance for stimuli presented in isolation and surrounded by flankers with an edge-to-edge spacing of ∼0.12′ (the smallest spacing tested across subjects). Single lines represent individual observers. Stimuli size was set as 3 times the size at threshold acuity for an isolated stimulus so that it was at ceiling levels in the isolated condition and acuity limits did not influence performance when stimuli were presented with surrounding flankers.

(B) An example of a one-frame presentation of a crowded stimulus rendered at threshold spacing on the cone mosaic for a single subject (subject S1). The cone locations under the stimulus are highlighted in green and those in between in red. For simplicity, we only considered a cone to be stimulated when the stimulus covered the cone center, thus excluding partial cone stimulation.

(C) Stimulus over the Voronoi grid of the cone mosaic for the same example observer (subject S1).

(D) Estimated thresholds (dashed lines) and psychometric fits across subjects. Edge-to-edge spacing is represented as multiple of each individual's average cone diameter in the stimulated region. The inset shows the same data but plotted as a function of flanker spacing defined in arcminutes. The filled black circle represents the average across subjects.

(E) Performance estimates derived from the psychometric fit are plotted against flanker spacings represented as multiples of cone diameter.

Error bars indicate ±1 SEM. The asterisks marks a statistically significant difference (* $p < 0.05$, ** $p < 0.01$, and *** $p < 0.001$).

(two-tailed paired t test, $t(5) = -7.66$, $p < 0.001$, $BF_{10} = 59.13$, Cohen's d = 1.38). These structural differences raise two key questions: first, does the extent of crowding change a few arcminutes away from the PRL where cone density is lower? Second, is the relationship between cone spacing and critical spacing preserved at larger foveolar eccentricities, or do cortical (or possibly retinal) pooling mechanisms increasingly drive the critical spacing even at small distances from the PRL?

Similarly to the first experiment, we scaled stimuli to 3× size thresholds determined by QUEST and tested varying flankers spacings while subjects maintained fixation on a central marker. Performance for isolated stimuli was near ceiling at both the PRL (0.99 ± 0.01) and 15′ from the PRL (0.98 ± 0.04), as shown in Figure 3F. Performance did not differ between the two locations ($t(5) = 0.86$, $p = 0.43$, $BF_{10} = 0.50$, Cohen's d = 0.34). As in the first experiment, we then identified the cones falling within the stimulus region and determined the average cone diameter. Figure 3G shows the behavioral performance as a function of target-flanker spacings expressed as multiples of cone diameter. We observed crowding spacing thresholds to increase on average by a factor of ∼3 (range: 0.74′ to 3.51′) at ∼15′ from the PRL, when

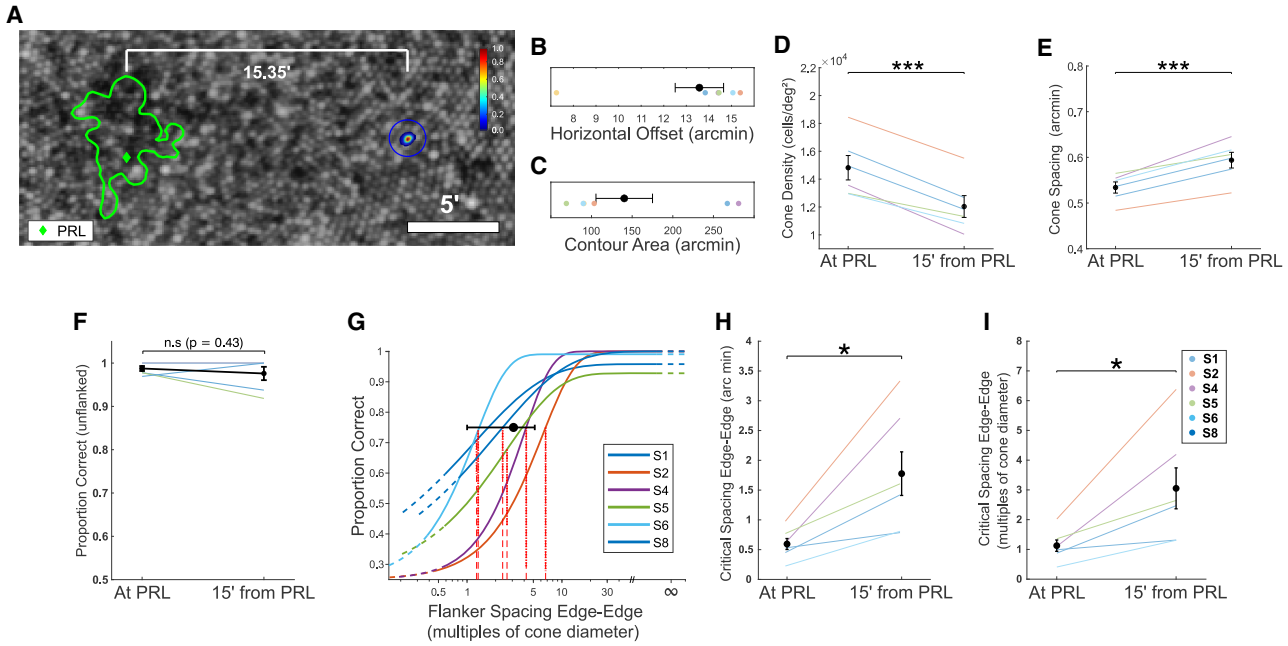

Figure 3. Critical spacing 15′ away from the PRL

(A) Stimuli were rendered approximately 15′ away from the PRL (green diamond with 68% contour map highlighted by the green trace for an example subject, subject S2). Stimuli were maintained at the same location with minimum variability. The heatmap shows the 2D distribution of the stimulated locations on the cone mosaic across trials.

(B) Horizontal offset of the median stimulus position from the PRL. Dots represent individual subjects. Subject S3 was excluded from subsequent analysis because their offset from the PRL was much smaller than the desired eccentricity.

(C) Average PRL 68% contour area across subjects. Dots represent individual observers.

(D) Cone density within the region stimulated at the PRL vs. 15′.

(E) Cone spacing within the stimulated region at the PRL vs. 15′. At 15′ from PRL, cone density was lower and cone spacing was larger than at the PRL.

(F) Unflanked performance at the PRL and 15′. Performance was near ceiling at both locations. Unflanked performance did not differ between the PRL and 15′.

(G–I) (G) Estimated thresholds (dashed lines) and psychometric fits across subjects. Edge-to-edge spacing is represented as multiples of each subject's average cone diameter within the stimulated region. Critical spacing estimates, or critical spacings, are represented as edge-to-edge separation in arcminutes in (H) and as edge-to-edge spacing in multiples of cone diameters in (I). Critical spacing was significantly larger at 15′ compared with the PRL when expressed in arcminutes and as multiples of cone diameters.

Single lines represent individual subjects. Error bars represent ±1 SEM. The asterisks mark statistically significant differences (* $p < 0.05$, ** $p < 0.01$, and *** $p < 0.001$).

See also Figure S3.

compared with thresholds obtained at the PRL. The average critical spacings were 1.79 ± 1.1, when represented in arcminutes, and 3.08 ± 2.08 times the cone diameter (see Figure S2 for individual psychometric functions).

When comparing spacing thresholds at the PRL and at ∼15′ from the PRL (Figures 3H and 3I), we observed that the critical spacing was larger in the latter condition. This was consistent when critical spacings were represented as E2E distance in arcminutes (two-tailed paired *t* test, $t(5) = 5.59$, $p = 0.019$, $BF_{10} = 4.28$, Cohen's d = 1.32) and as multiples of cone diameter (two-tailed paired *t* test, $t(5) = 5.11$, $p = 0.03$, $BF_{10} = 3.37$, Cohen's d= 1.13) (Figures 3H and 3I) (see also Figure S3A showing thresholds in nominal values, and Figure S3B as center-to-center separations in multiples of cone diameter). Hence, this increase in thresholds cannot be attributed solely to increased cone spacing at the larger eccentricity, which increased from 0.53′ ± 0.03′ to 0.59′ ± 0.04′. Importantly, the effect persisted when we excluded the two participants showing the largest change (Subjects S2 and S4) (center to center in cone diameters: $t(3) = -3.75$, $p = 0.033$, $BF_{10} = 3.16$, Cohen's d = 1.28; edge to edge in arcminutes: $t(3) = -4.23$, $p = 0.024$, $BF_{10} = 3.89$, Cohen's d = 1.42). These results show that just 15′ away from the PRL the one-to-one relationship between cone diameter and critical spacings is no longer present; critical spacings were significantly larger than the cone diameter at this eccentricity. Such discrepancy between cone spacing and critical spacings just a few arcminutes away from the PRL suggests the presence of larger pooling regions, likely at the cortical level, at this eccentricity. We observed considerable individual variability in critical spacing thresholds, both at the PRL and at 15′ eccentricity (Figure S2), a variability not mirrored in cone density. A positive, though not statistically significant, Spearman correlation between PRL and peri-PRL thresholds across subjects ($\rho = 0.77$, $p = 0.081$) suggests that some of the variability reflects subject-level traits that generalize across nearby eccentricities rather than purely local structural differences.

We then compared our E2E critical spacing estimates with midget RGC (mRGC) spacing based on Watson's model[84] to examine whether retinal factors could explain the observed increase in critical spacing (Figure 4A). This comparison indicated

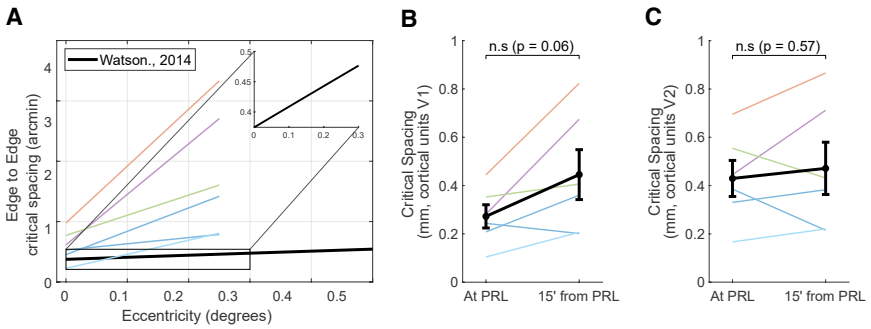

Figure 4. Retinal and cortical mapping of critical spacing

(A) Edge-to-edge critical spacing across eccentricity compared with predicted midget RGC (mRGC) spacing from Watson's model.[84] Dashed lines show individual subjects at the PRL (0°) and 15 ′ (0.25°); the solid black line shows the model prediction. The inset provides an expanded view of the 0°–0.25° range. The divergence between subject-derived critical spacing and the model prediction indicates increasing cortical pooling with eccentricity. The slope of subject-derived critical spacing between 0° and 0.25° was significantly steeper than that predicted by the model.

(B and C) Critical spacing converted to cortical distance (mm) using (Schira et al.[86]) cortical magnification for V1 (B) and V2/V3 (C). Single lines represent individual subjects. Error bars represent ±1 SEM.

that while critical spacing at the PRL was only slightly larger than the mRGC spacing estimates, at 15′ (0.25°) it was considerably larger, suggesting that cortical pooling may contribute more strongly to crowding at greater eccentricities. Additionally, the slope of the subject-derived critical spacing between these eccentricities was statistically higher compared with the slope predicted by the mRGC spacing (paired t test, $t(5) = 3.17$, $p = 0.025$, $BF_{10} = 2.20$, Cohen's d = 1.30), supporting the interpretation of larger cortical pooling regions at this scale. As a complementary test, we then asked whether cortical scaling could account for the eccentricity effect by converting our critical spacing estimates into cortical distance using a standard cortical magnification function (see STAR Methods for details). Following the procedure outlined by Strasburger,[85] we estimated cortical critical spacing (κ) based on foveal parameters from Schira et al.,[86] combined with psychophysically derived $\widehat{E}2$ values from our dataset. When expressed in cortical units using V1 parameters ($M0 = 28$ mm/°, $E_2 = 0.312°$), critical spacing showed only a trend toward increase at 0.25° eccentricity ($t(5) = -2.39$, $p = 0.062$, $BF_{10} = 1.78$, Cohen's d = 0.74), as illustrated in Figure 4B. In contrast, when using V2 parameters ($M_0 = 45$ mm/°, $E_2 = 0.147°$), the relationship flattened, yielding constant spacing across subjects ($t(5) = -0.61$, $p = 0.568$, $BF_{10} = 0.43$, Cohen's d = 0.15, as shown in Figure 4C. These results suggest that cortical magnification in V2 can largely account for the eccentricity-dependent increase in critical spacing, consistent with previous neuro-imaging results showing that crowding effects correlate with population receptive field size in V2.[87] At the same time, because critical spacing at 15′ (0.25°) already exceeds mRGC separation, these results are consistent with the possibility that additional pooling beyond retinal sampling plays a role within the foveola.

Mislocalization errors at the PRL vs. larger foveolar eccentricities

When stimuli are crowded, the presence of surrounding flankers can alter the perceived location of the target object. Mislocalization is particularly strong at slightly larger extrafoveal eccentricities, where it occurs due to increased positional uncertainty, leading individuals to incorrectly report one of the flanking objects instead of the target—a phenomenon known as a mislocalization error.[42–44] In a 4 alternate forced choice task (4-AFC task), there are three other possible options for an incorrect response, corresponding to a mislocalization guess rate of 33%. If the probability of responding to one of the flankers is higher than the guess rate, it indicates a bias toward one of the flanker locations (see example for stimuli presented at the PRL in Figure 5A and when presented 15′ to the right of the PRL in Figure 5B). Here, we examined whether mislocalization is present at the PRL, where the flankers are equidistant from the PRL, and whether a specific pattern emerges at 15′, providing insight into positional biases at this eccentricity.

Figure 5C shows that for stimuli that were stabilized at a retinal location ∼ 15′ from the PRL, there was a significant interaction between eccentricity and mislocalization type (repeated measures ANOVA: $F(1,5) = 51.413, p_{GG} < 0.00$). Mauchly's test indicated a violation of sphericity $(W = 0.020, \chi^2(5) = 14.53, p = 0.013)$, but applying the Greenhouse-Geisser correction did not change the significance pattern. Post hoc analysis using the Tukey-Kramer test revealed that the difference in bias between the leftward and rightward flanker locations was significant at 15′ eccentricity ($p = 0.031$), while no statistically significant difference was observed at the PRL ($p = 0.105$). Similar results were obtained at the PRL when the stimulus was presented without retinal stabilization. Moreover, we did not find a statistically significant difference between the stabilized condition at the PRL and the unstabilized condition (repeated measures ANOVA: $F(1,7) = 0.269$, $p_{GG} = 0.62$) (Figure S4A). Thus, for stimuli presented 15′ from the PRL, individuals were more likely to report the inner or leftward flanker location on incorrect trials—the one closer to the PRL.

Experiment 3: Influence of FEMs

In the current study, we stabilized the stimulus at the PRL to ensure that we targeted the same set of cones between trials to better understand the interplay between cone diameter and critical spacing estimates. Normally, however, ocular drift moves the projection of the fixated stimulus over many photoreceptors during the course of fixation.[14,63,65–68] Visual acuity and fine spatial vision are modulated by ocular drift.[60,61,65,80] The retinal motion introduced by ocular drift is beneficial for acuity and fine spatial vision.[62,63,66,88,89] In particular, it has been shown that when the temporal modulations of ocular drift are removed, either using retinal stabilization or brief stimuli presentation, acuity and performance in fine discrimination tasks drop.[60,62,66] Further, ocular drift has been shown to increase critical spacing in natural viewing conditions (i.e., without stabilization).[14] Because crowding pooling regions are the smallest at the center of gaze, ocular drift effectively moves target and flankers over different pooling

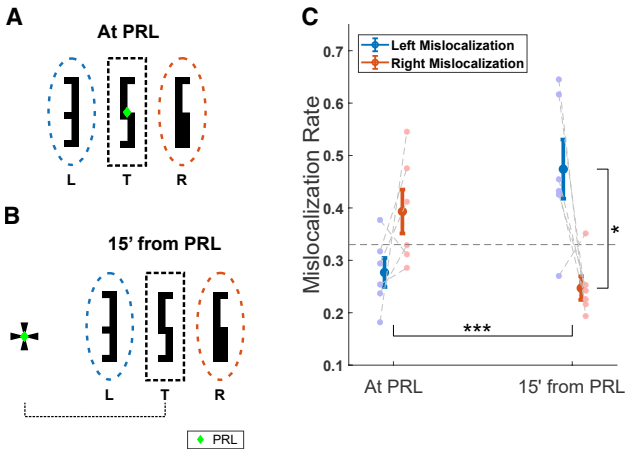

Figure 5. Mislocalization errors across viewing condition

(A and B) Schematic illustration of the crowded stimulus at two retinal locations: (A) at the PRL and (B) 15′ to the right of the PRL. In (A), the target is centered at the PRL and highlighted by a black dashed square. In (B), a Maltese cross (5′ × 5′) was shown to aid fixation, while the target was presented to the right of the PRL. Leftward and rightward flankers are marked by blue and orange dashed ovals, respectively. The PRL (green diamond) is shown for an example subject.

(C) Average probability of responding to one of the two flanker locations (inner and outer) on incorrect trials are plotted for each subject for trials, where the stimulus was stabilized at the PRL and at a retinal location 15′ to the right of the PRL. At 15′ eccentricity, observers showed a stronger bias toward the inner (leftward) flanker, the one closer to the PRL. At the PRL, responses were similar between the inner and outer mislocalizations, indicating no directional bias. Single dots represent individual observers. Error bars represent ±1 SEM. The asterisks denote significant main effects and post hoc comparisons (* $p < 0.05$, ** $p < 0.01$, and *** $p < 0.001$).

See also Figure S4A.

regions, and it may lead to the same pooling region being stimulated by both target and flanker over time. To further examine the impact of ocular drift on crowding and to determine the extent to which the flanker and target stimulate the same photoreceptors over time, a separate experiment (experiment 3) was conducted. In this experiment, stimuli were maintained at a fixed location in physical space (i.e., on the imaging raster), but due to ocular drift, their retinal location varied over time.

A QUEST procedure was used to first determine the threshold stimulus size when the stimulus was viewed in isolation without retinal stabilization. Consistent with previous work presenting stimuli at the PRL in the presence of habitual optical imperfections of the eye,[14] and with work presenting stimuli using AOSLO to correct for optical aberrations at 0.8°–1.3° from the PRL,[66] we found that visual acuity thresholds dropped (i.e., higher acuity) by 0.43′ ± 0.09′ (23% reduction) when stimuli were not retinally stabilized (see Figure S4B). Figure 6A shows the 2D stimulus probability distribution map on the retina as a result of ocular drift for an example subject. On average, the Euclidean distance between the median of stimulus locations and the PRL was found to be 2.29′ ± 3.53′ (see Figure S5 for individual stimulus distribution maps). In the crowded condition, the stimulus size was maintained at a constant size that was three times the threshold size measured in isolation. Critical spacing estimates were found to range between 0.46′ to 1.90′ (see Figure 6B). On average, the critical spacing was 0.98′ ± 0.46′ (see Figure S2 for individual psychometric functions).

To gain insights into the respective contributions of optical aberrations and FEMs to foveal crowding, we compared our critical spacing thresholds with a previous study that used a similar stimulus design.[14] To this end, we re-computed E2E thresholds at 62.5% correct for a 4-AFC task to match the convention in Clark et al.[14] (see Figure S6). Although critical spacing was on average larger in Clark et al.[14] (0.93′ ± 0.64′) compared with the unstabilized condition in the current study (0.63′ ± 0.26′), this difference was not statistically significant (Wilcoxon rank sum, W =57, p = 0.463), suggesting that crowding is little influenced by the optical quality of the stimulus, provided the stimulus size is above the acuity threshold. In contrast, critical spacing was reduced under stabilization from the current study (0.38′ ± 0.17′) relative to Clark et al.[14] (Wilcoxon rank sum, W = 41, p = 0.006), indicating that FEMs are the dominant factor influencing foveal crowding, with optical factors playing a lesser role.

Consistent with Clark et al.,[14] we observed a systematic increase in critical spacing thresholds, when expressed as E2E spacing, without retinal stabilization when compared with the stabilized condition at the PRL (two-tailed paired t test, $t(7)$ = −3.11, p = 0.02, BF_{10} = 4.29, Cohen's d = 0.94) (Figure 6C).

Figure 6D shows the average probability of each cone being stimulated by the array of digits for an example subject, for stimuli presented under retinal stabilization, and for unstabilized stimuli (Figure 6E). Note that, ideally, retinal stabilization should limit stimulation to the same subset of cones throughout stimulus exposure, yet perfect stabilization is technically impossible to achieve and tiny residual errors are always present, resulting in a small number of neighboring cones being stimulated. In contrast, in the unstabilized condition, the stimulus is swept over many photoreceptors, as shown in Figure 6E. Even if target and flankers stimulate different cones and pooling region, when moved across the retina by ocular drift the same cones/pooling regions may be stimulated by both. To determine the probability of this happening we calculated the average probability of a cone stimulated by the target to be also stimulated by either of the flankers during a trial (see STAR Methods for details). As expected, Figure 6F shows that the probability of shared stimulation was higher in the unstabilized condition (0.40 ± 0.21) ($t(5)$ = −5.53, p = 0.003, BF_{10} = 18.93, Cohen's d = 2.27) when compared with the stabilized condition (0.02 ± 0.04).

Taken together, these findings are consistent with the idea that although drift motion improves visual acuity in the unstabilized condition, in the task examined here it exacerbates the crowding effect likely because there is a higher probability that target and flankers stimulate the same crowding pooling region over time, increasing uncertainty in the identification of the target.[14]

DISCUSSION

Crowding is a fundamental aspect of visual perception as it affects object recognition. Although this phenomenon is primarily studied in the visual periphery, it also impacts foveal vision.[9–15] It has been suggested that the extent of crowding reflects the number of cortical neurons per degree squared involved in visual recognition.[9,58] Thus, determining the critical spacing achievable in the fovea—once confounding factors are

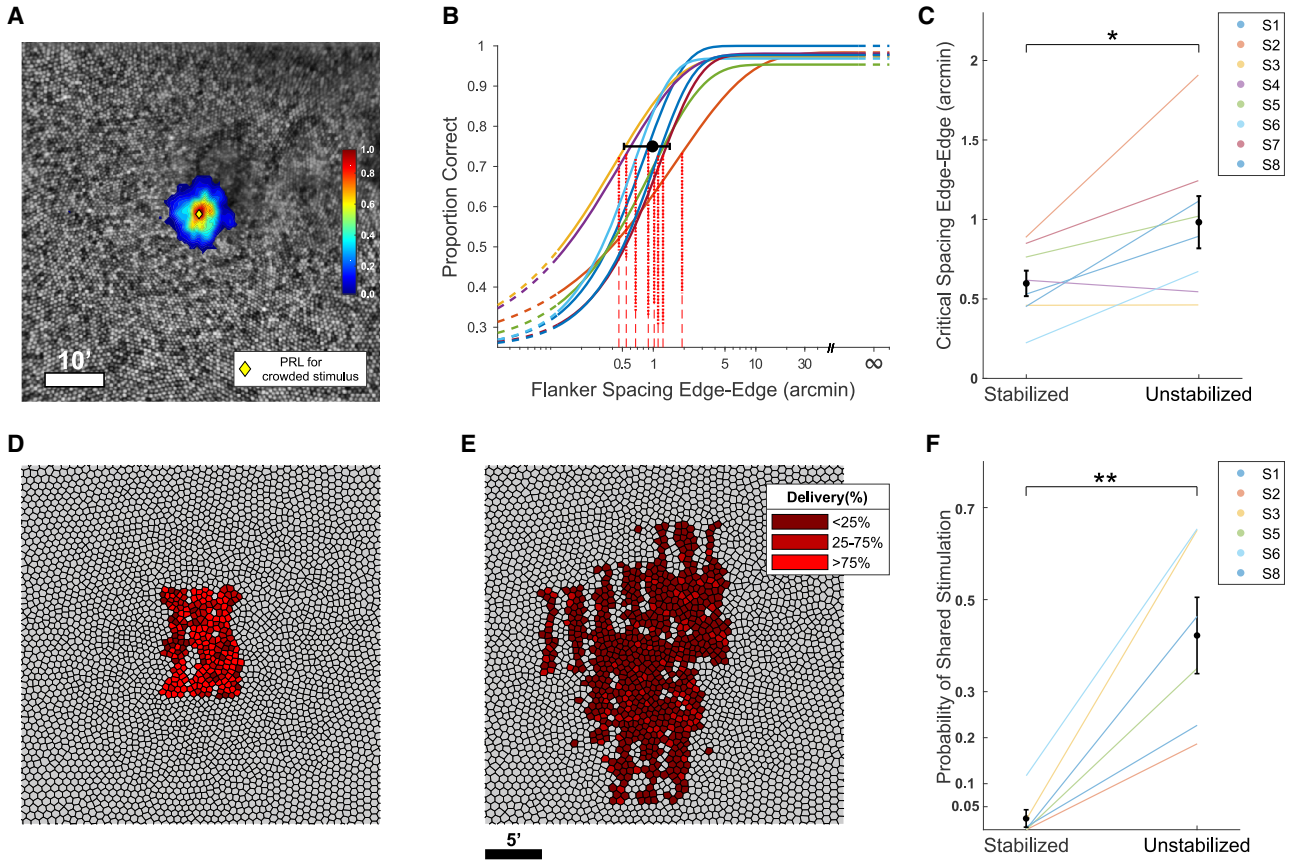

Figure 6. Critical spacing for unstabilized viewing condition

(A) Normalized 2D distribution of stimulus positions on the retina across trials during unstabilized viewing for an example subject (subject S1).

(B) Estimated edge-to-edge spacing thresholds (dashed lines) and individual psychometric fits for the unstabilized condition. The filled black circle represents the average across subjects.

(C–E) (C) Average critical spacing thresholds in the stabilized and unstabilized conditions. Critical spacing thresholds were larger in the unstabilized condition than in the stabilized condition at the PRL. Probability of cone stimulation in single trial (15 frames) under stabilized (D) and unstabilized (E) viewing, respectively, for subject S1.

(F) The probability of a cone being stimulated by the target and either of the flankers over the course of stimulus presentation in the stabilized and the unstabilized condition when the stimulus is presented at the PRL. The probability of shared stimulation was higher in the unstabilized condition than in the stabilized condition at the PRL.

Single lines represent individual subjects. Error bars represent ±1 SEM. The asterisks mark statistically significant differences (* $p < 0.05$, ** $p < 0.01$, and *** $p < 0.001$).

See also Figures S4B, S5, and S6.

accounted for—could provide key insights into the cortical representation of stimuli across the foveola. Additionally, given how important foveal vision is for daily activities from reading to driving, it is critical to unravel the mechanisms underlying foveal crowding and to shed light on whether they differ from those affecting extrafoveal vision. Measuring critical spacings at the foveal scale is challenging; in order to study crowding effects, stimuli need to be above the acuity limit (yet not too large, otherwise crowding is not observed), and standard optotypes are not ideal for testing critical spacing in the central fovea.[9] Further, the inherent optical aberrations of the eye scatter the incoming light posing another limitation to assessing critical spacing. Finally, the ever-present ocular drift has an impact on visual crowding,[14] acting as an additional confounding factor when testing crowding at this scale. Here, to eliminate these confounds, we used stimuli above the acuity limit, and we used stimuli in Pelli's font, which has been specifically designed to test the smaller critical spacings.[9]

Previous studies[10,16] observed facilitation at the closest spacing tested with bar stimuli, E's or Landolt C's, which, when brought close together, form a Gestalt that makes it easier to identify the target orientation. In our study however, we do not report facilitation effects for the smaller spacings. This is likely due to the stimuli, digits in Pelli's font, and type of task, digit identification instead of orientation discrimination, used here; performance progressively decreased with decreasing spacing, even with the smallest spacing tested (~0.12′ and even 0′ or abutting for one subject). Hence, the findings from the current study further validate the utility of using Pelli's font for studying foveal crowding[9]; by avoiding facilitation effects at the smaller spacing, by presenting stimuli above the acuity threshold, and by controlling for optical spreading and eye movements, we can effectively assess the

limits of crowding extent at the foveal scale. Compared with prior work, our critical spacing thresholds were lower overall. Among studies using similar digit stimuli, Pelli et al.[9] reported larger thresholds, whereas Clark et al.[14] reported thresholds similar to ours in the unstabilized condition (experiment 3). The higher values reported by Pelli et al.[9] likely reflect the nine-digit response set (1–9) and the resulting lower guess rate, as well as the absence of trial-discarding criteria based on FEMs and fixation precision. By contrast, Danilova and Bondarko[90] and Lev et al.[91] used tumbling-E targets flanked by tumbling-E, which yielded larger critical spacing thresholds. Differences in stimulus design, response set, and threshold definitions (for example, E2E vs. center-to-center spacing and performance criterion) make direct cross-study comparisons challenging.

Our findings indicate that, at the PRL, the critical spacings for stimuli under retinal stabilization, when measured as E2E separation, closely match the average cone diameter in the stimulated region. Such critical spacing leads to a substantial drop in performance (~25% from the asymptotic level). A less pronounced drop in performance is present when spacing covers about two cones, in which case, on average subjects can still perform the task with high accuracy (~90% correct responses on average). Notably, our critical spacing estimates are much smaller than those reported in previous work,[10] as expected when examining crowding extent controlling for factors that can inflate these estimates. Although our estimates may appear smaller also compared with those reported previously[16] when correcting for optical aberrations, a fair comparison cannot be drawn due to the smaller stimuli size used in their study, which was closer to the acuity limit, and their reported rebound effect in performance when using smaller spacings. Interestingly, the critical spacing thresholds reported here are also much smaller than the Ricco's area, the region over which light at detection threshold on the photoreceptors is fully pooled by the visual system,[92] coherent with the idea that crowding and contrast sensitivity are mediated by different mechanisms.

Despite its importance, little is known about whether and how visual functions and neural mechanisms are modulated across the central fovea. In contrast, peripheral crowding has been better characterized, and from 4 ° to 18.5 ° it has been shown that crowding zones cover approximately the same number of RGCs.[33] Studying vision at this scale is difficult as receptors are tightly packed and neurons have the smallest receptive fields, making it difficult to record neural activity at different foveolar eccentricities, and, with a few exceptions,[86,93] neural imaging techniques do not have the spatial resolution to image neural activity at this finer grain. Further, FEMs constantly move the stimulus across many receptors making it difficult to limit visual stimulation at a desired foveolar eccentricity. This study bridges some of these knowledge gaps by providing a window into the mechanisms controlling visual crowding at this scale and how they vary across the foveola. Although the central fovea covers only 1° of visual angle, it has been shown that fine spatial vision within this tiny region is not homogeneous,[56,60] yet other visual functions, such as spot-light sensitivity, have been shown to be uniform across the foveola.[55] It has also been speculated that the effects of crowding are the same across the central fovea.[3] Still, because of technical difficulties, this has never been tested. Addressing this problem can provide crucial insights into how visual information and object recognition processes operate at this scale.

Our results show that pooling mechanisms begin to play a larger role with increasing eccentricity, even at this fine scale. Near the PRL, critical spacings closely matched cone diameter estimates, indicating minimal influence from neural pooling mechanisms. However, just a few arcminutes away from the PRL, additional neural pooling factors influenced critical spacings. At which level does this signal pooling occur? It is possible that divergence (i.e., 1 cone to 2 mRGCs) within the central fovea is not complete and some reduction in divergence starts to occur already at 0.25° eccentricity. Cortical magnification, which inherits its structure from retinal architecture,[27,94] could provide the framework for spatial integration. Yet, it is debated whether RGC density fully accounts for the cortical magnification factor in V1 and beyond. Although previous work suggests that there is not a selective amplification of the foveal representation cortically,[27] other work has suggested otherwise[95–98]; the cortical representation of the central visual field is amplified beyond the magnification expected from RGC density. In line with this, we find that that critical spacing at 15′ (0.25°) exceeded mRGC spacing predicted by the Watson model and increased more steeply with eccentricity,[84] indicating that retinal sampling and possibly increasing convergence between cones and RGCs at 0.25° eccentricity are not sufficient. They also align with high-resolution fMRI studies reporting a gradient in cortical magnification in both humans and non-human primates.[86,93]

Based on the pooling theory of crowding, the visual system integrates information from neighboring regions, which for crowded stimuli affects the perceived positions of the target and flankers[42–44] leading to mislocalization errors, i.e., subjects report either one of the flankers instead of the target stimulus. Extrafoveally, some studies have observed an increased tendency to respond to the outer flanker, as it is believed to have a stronger impact on object recognition.[1,99] In contrast, other studies have observed the opposite pattern, with a greater bias toward the inner flanker.[100,101] Here, we find that at the very center of gaze, when both flankers are approximately equidistant from the PRL, whether or not retinal stabilization is used, there is no bias toward a specific flanker location, i.e., mislocalization errors do not occur. However, when stimuli were presented 15′ to the right of the PRL, we observed a bias in reporting the leftward flanker, which is the flanker closer to the PRL, when identifying the target. This tendency could be the result of crowding pooling regions being elongated in the direction of the PRL at this foveolar eccentricity, yet further research is necessary to determine whether this is the case. Remarkably, although mislocalization errors have often been reported with the visual crowding effect in the peripheral visual field, here we observe a similar pattern at eccentricities just a few arcminutes away from the PRL, further suggesting an increased impact of cortical pooling factors with increasing foveolar eccentricity. Further, the absence of mislocalization errors at the PRL suggests that crowding mechanisms function differently than in the region immediately surrounding the PRL.

Although ocular drift moves stimuli across several cone photoreceptors within the fovea,[65,102] this movement has been shown to benefit high-acuity tasks.[60,61] In contrast, retinally stabilizing stimuli results in decreased performance in high-acuity

tasks.[14,60,66] Although beneficial for visual acuity tasks, these drifts negatively impact performance in cluttered scenarios when the target is surrounded by distractors.[14] Consistent with previous findings,[14] we observed an increase in the critical spacing in the absence of retinal stabilization, suggesting that although drift motion improves acuity, it exacerbates the visual crowding effect in these conditions when target and flankers cannot be grouped/un-grouped into a Gestalt. This likely results from a higher probability that the targets and flankers stimulate the same crowding pooling region over time, increasing the uncertainty in target identification.

It is important to note that although crowding is often viewed as a phenomenon that hinders acuity, it may often be advantageous in natural conditions. In fact, it facilitates perception and extraction of patterns from the visual input,[7,103–105] and it can be considered a mechanism for efficient exploitation of spatial redundancies of the natural world.[106] It has been shown that Gestalt grouping can alleviate the negative effects of crowding by perceptually separating the target from surrounding elements, thus reducing interference.[107,108] Crowding at the foveal scale likely serves a similar role; given that the foveal input is often rich in details forming a Gestalt and visual textures, the mechanisms underlying crowding, together with the beneficial effects of drift on acuity may aid fine texture discrimination and grouping of shapes into a coherent structure. Foveal crowding mechanisms, on the other hand, are likely a hindrance when reading small characters (e.g., reading highway driving directions from a distance).

In summary, using state-of-the-art retinal imaging and retinal-contingent stimulus rendering to eliminate influences of optical scattering and FEMs, we demonstrated that the critical spacing of foveal crowding at the PRL approximately matches with photoreceptoral spacing, showing that it is either driven by pre-cortical factors or that cortical pooling regions are close to the size of a single photoreceptor. Just 15′ off the PRL, however, we observed a divergence from these characteristics, suggesting that additional cortical mechanisms start to influence crowding even within the foveola. Furthermore, mislocalization errors were more biased toward the flanker positioned closer to the PRL for stimuli presented 15′ away, with no apparent bias observed at the PRL, indicating that the underlying mechanisms of crowding may differ between the PRL and other eccentricities. These findings revealed that while crowding extent (under diffraction-limited viewing) is predicted by photoreceptor spacing at the PRL, only 0.25° off the PRL, the broader foveola is influenced by further cortical pooling. This study provides a new understanding of crowding mechanisms, and of the mechanisms underlying visual processing in the central fovea, and underscores the importance of considering both eye movements and retinal structure when examining visual functions at this scale.

RESOURCE AVAILABILITY

Lead contact

Requests for further information and resources should be directed to and will be fulfilled by the lead contact, Krishnamachari S. Prahalad (pkrishn5@ur.rochester.edu).

Materials availability

This study did not generate new unique reagents.

Data and code availability

- Human behavioral data have been deposited at https://osf.io/yugdj and are publicly available as of the date of publication.
- All original code has been deposited at https://osf.io/yugdj and is publicly available as of the date of publication.
- Any additional information required to reanalyze the data reported in this paper is available from the lead contact upon request.

ACKNOWLEDGMENTS

This work was supported by the National Institutes of Health grant EY029788 (to M.P.), R01 EY018363 (to M.R.), EY001319 (to the Center for Visual Science), R01 EY023591 (to A.R.), and Ha5323/6-1 and Ha5323/8-1 (to W.H.). We would also like to thank Dr. Daniel Coates for their helpful discussions in the experimental design and analysis.

AUTHOR CONTRIBUTIONS

K.S.P., M.P., A.M.C., and B.M. designed the study. K.S.P., B.M., S.K.J., S.K., and A.M.C. collected the data. K.S.P. and M.P. analyzed the data. K.S.P. and M.P. wrote the manuscript with input from all authors.

DECLARATION OF INTERESTS

The authors declare no competing interests.

STAR★METHODS

Detailed methods are provided in the online version of this paper and include the following:

SUPPLEMENTAL INFORMATION

Supplemental information can be found online at https://doi.org/10.1016/j.cub.2025.11.007.

Received: June 17, 2025
Revised: September 29, 2025
Accepted: November 4, 2025
Published: December 2, 2025

REFERENCES

1. Bouma, H. (1970). Interaction effects in parafoveal letter recognition. Nature *226*, 177–178. https://doi.org/10.1038/226177a0.

2. Stuart, J.A., and Burian, H.M. (1962). A Study of Separation Difficulty: Its Relationship to Visual Acuity in Normal and Amblyopic Eyes. Am. J. Ophthalmol. *53*, 471–477. https://doi.org/10.1016/0002-9394(62)94878-X.
3. Toet, A., and Levi, D.M. (1992). The two-dimensional shape of spatial interaction zones in the parafovea. Vis. Res. *32*, 1349–1357. https://doi.org/10.1016/0042-6989(92)90227-A.
4. Levi, D.M. (2008). Crowding—An essential bottleneck for object recognition: A mini-review. Vis. Res. *48*, 635–654. https://doi.org/10.1016/j.visres.2007.12.009.
5. Pelli, D.G., and Tillman, K.A. (2008). The uncrowded window of object recognition. Nat. Neurosci. *11*, 1129–1135. https://doi.org/10.1038/nn.2187.
6. Strasburger, H., Harvey, L.O., and Rentschler, I. (1991). Contrast thresholds for identification of numeric characters in direct and eccentric view. Percept. Psychophys. *49*, 495–508. https://doi.org/10.3758/BF03212183.
7. Strasburger, H., Rentschler, I., and Jüttner, M. (2011). Peripheral vision and pattern recognition: A review. J. Vis. *11*, 13. https://doi.org/10.1167/11.5.13.
8. Song, S., Levi, D.M., and Pelli, D.G. (2014). A double dissociation of the acuity and crowding limits to letter identification, and the promise of improved visual screening. J. Vis. *14*, 3. https://doi.org/10.1167/14.5.3.
9. Pelli, D.G., Waugh, S.J., Martelli, M., Crutch, S.J., Primativo, S., Yong, K.X., Rhodes, M., Yee, K., Wu, X., Famira, H.F., and Yiltiz, H. (2016). A clinical test for visual crowding. F1000Res *5*, 81. https://doi.org/10.12688/f1000research.7835.1.
10. Flom, M.C., Weymouth, F.W., and Kahneman, D. (1963). Visual Resolution and Contour Interaction. J. Opt. Soc. Am. *53*, 1026–1032. https://doi.org/10.1364/JOSA.53.001026.
11. Coates, D.R., and Levi, D.M. (2014). Contour interaction in foveal vision: a response to siderov, waugh, and bedell (2013). Vis. Res. *96*, 140–144. https://doi.org/10.1016/j.visres.2013.10.016.
12. Siderov, J., Waugh, S.J., and Bedell, H.E. (2013). Foveal contour interaction for low contrast acuity targets. Vis. Res. *77*, 10–13. https://doi.org/10.1016/j.visres.2012.11.008.
13. Bondarko, V.M., Chikhman, V.N., Danilova, M.V., and Solnushkin, S.D. (2024). Foveal crowding for large and small Landolt Cs: Similarity and Attention. Vis. Res. *215*, 108346. https://doi.org/10.1016/j.visres.2023.108346.
14. Clark, A.M., Huynh, A., and Poletti, M. (2024). Oculomotor Contributions to Foveal Crowding. J. Neurosci. *44*, e0594242024. https://doi.org/10.1523/JNEUROSCI.0594-24.2024.
15. Shamsi, F., Liu, R., and Kwon, M. (2022). Foveal crowding appears to be robust to normal aging and glaucoma unlike parafoveal and peripheral crowding. J. Vis. *22*, 10. https://doi.org/10.1167/jov.22.8.10.
16. Coates, D.R., Levi, D.M., Touch, P., and Sabesan, R. (2018). Foveal Crowding Resolved. Sci. Rep. *8*, 9177. https://doi.org/10.1038/s41598-018-27480-4.
17. Boycott, B.B., Dowling, J.E., and Kolb, H. (1969). Organization of the Primate Retina: Light Microscopy. Philos. Trans. R. Soc. Lond. B *255*, 109–184.
18. Calkins, D.J., Schein, S.J., Tsukamoto, Y., and Sterling, P. (1994). M and L cones in macaque fovea connect to midget ganglion cells by different numbers of excitatory synapses. Nature *371*, 70–72. https://doi.org/10.1038/371070a0.
19. Kolb, H., and Marshak, D. (2003). The midget pathways of the primate retina. Doc. Ophthalmol. *106*, 67–81. https://doi.org/10.1023/A:1022469002511.
20. Polyak, S.L. (1941). The Retina (University of Chicago Press).
21. Crossland, M.D., Culham, L.E., Kabanarou, S.A., and Rubin, G.S. (2005). Preferred Retinal Locus Development in Patients with Macular Disease. Ophthalmology *112*, 1579–1585. https://doi.org/10.1016/j.ophtha.2005.03.027.
22. Guez, J.E., Le Gargasson, J.F., Rigaudiere, F., and O'Regan, J.K. (1993). Is there a systematic location for the pseudo-fovea in patients with central scotoma? Vis. Res. *33*, 1271–1279. https://doi.org/10.1016/0042-6989(93)90213-G.
23. Curcio, C.A., Sloan, K.R., Kalina, R.E., and Hendrickson, A.E. (1990). Human photoreceptor topography. J. Comp. Neurol. *292*, 497–523. https://doi.org/10.1002/cne.902920402.
24. Jing, W., Liu, W.-Z., Gong, X.-W., Gong, H.-Q., and Liang, P.-J. (2010). Visual pattern recognition based on spatio-temporal patterns of retinal ganglion cells' activities. Cogn. Neurodyn. *4*, 179–188. https://doi.org/10.1007/s11571-010-9119-8.
25. Drasdo, N. (1977). The neural representation of visual space. Nature *266*, 554–556. https://doi.org/10.1038/266554a0.
26. Hubel, D.H., and Wiesel, T.N. (1974). Uniformity of monkey striate cortex: A parallel relationship between field size, scatter, and magnification factor. J. Comp. Neurol. *158*, 295–305. https://doi.org/10.1002/cne.901580305.
27. Wässle, H., Grünert, U., Röhrenbeck, J., and Boycott, B.B. (1990). Retinal ganglion cell density and cortical magnification factor in the primate. Vis. Res. *30*, 1897–1911. https://doi.org/10.1016/0042-6989(90)90166-I.
28. Van Essen, D.C., Newsome, W.T., and Maunsell, J.H.R. (1984). The visual field representation in striate cortex of the macaque monkey: Asymmetries, anisotropies, and individual variability. Vis. Res. *24*, 429–448. https://doi.org/10.1016/0042-6989(84)90041-5.
29. Tootell, R.B.H., Silverman, M.S., Switkes, E., and De Valois, R.L. (1982). Deoxyglucose Analysis of Retinotopic Organization in Primate Striate Cortex. Science *218*, 902–904. https://doi.org/10.1126/science.7134981.
30. Cowey, A., and Rolls, E.T. (1974). Human cortical magnification factor and its relation to visual acuity. Exp. Brain Res. *21*, 447–454. https://doi.org/10.1007/BF00237163.
31. Kolb, H., Nelson, R.F., Ahnelt, P.K., Ortuño-Lizarán, I., and Cuenca, N. (1995). The Architecture of the Human Fovea. In Webvision: The Organization of the Retina and Visual System, H. Kolb, E. Fernandez, and R. Nelson, eds.
32. Rossi, E.A., and Roorda, A. (2010). The relationship between visual resolution and cone spacing in the human fovea. Nat. Neurosci. *13*, 156–157. https://doi.org/10.1038/nn.2465.
33. Kwon, M., and Liu, R. (2019). Linkage between retinal ganglion cell density and the nonuniform spatial integration across the visual field. Proc. Natl. Acad. Sci. USA *116*, 3827–3836. https://doi.org/10.1073/pnas.1817076116.
34. Coates, D.R., Jiang, X., Levi, D.M., and Sabesan, R. (2022). Cortical distance unifies the extent of parafoveal contour interactions. J. Vis. *22*, 15. https://doi.org/10.1167/jov.22.2.15.
35. Anderson, E.J., Dakin, S.C., Schwarzkopf, D.S., Rees, G., and Greenwood, J.A. (2012). The Neural Correlates of Crowding-Induced Changes in Appearance. Curr. Biol. *22*, 1199–1206. https://doi.org/10.1016/j.cub.2012.04.063.
36. Millin, R., Arman, A.C., Chung, S.T.L., and Tjan, B.S. (2014). Visual Crowding in V1. Cereb. Cortex *24*, 3107–3115. https://doi.org/10.1093/cercor/bht159.
37. Freeman, J., and Simoncelli, E.P. (2011). Metamers of the ventral stream. Nat. Neurosci. *14*, 1195–1201. https://doi.org/10.1038/nn.2889.
38. He, S., Cavanagh, P., and Intriligator, J. (1996). Attentional resolution and the locus of visual awareness. Nature *383*, 334–337. https://doi.org/10.1038/383334a0.
39. Intriligator, J., and Cavanagh, P. (2001). The spatial resolution of visual attention. Cogn. Psychol. *43*, 171–216. https://doi.org/10.1006/cogp.2001.0755.
40. Taylor, S.G., and Brown, D.R. (1972). Lateral visual masking: Supraretinal effects when viewing linear arrays with unlimited viewing time. Percept. Psychophys. *12*, 97–99. https://doi.org/10.3758/BF03212851.
41. Tripathy, S.P., and Levi, D.M. (1994). Long-range dichoptic interactions in the human visual cortex in the region corresponding to the

blind spot. Vis. Res. *34*, 1127–1138. https://doi.org/10.1016/0042-6989(94)90295-X.

42. Greenwood, J.A., Bex, P.J., and Dakin, S.C. (2009). Positional averaging explains crowding with letter-like stimuli. Proc. Natl. Acad. Sci. USA *106*, 13130–13135. https://doi.org/10.1073/pnas.0901352106.
43. Parkes, L., Lund, J., Angelucci, A., Solomon, J.A., and Morgan, M. (2001). Compulsory averaging of crowded orientation signals in human vision. Nat. Neurosci. *4*, 739–744. https://doi.org/10.1038/89532.
44. Pelli, D.G., Palomares, M., and Majaj, N.J. (2004). Crowding is unlike ordinary masking: Distinguishing feature integration from detection. J. Vis. *4*, 1136–1169. https://doi.org/10.1167/4.12.12.
45. Haberman, J., and Whitney, D. (2007). Rapid extraction of mean emotion and gender from sets of faces. Curr. Biol. *17*, R751–R753. https://doi.org/10.1016/j.cub.2007.06.039.
46. Dakin, S.C., Cass, J., Greenwood, J.A., and Bex, P.J. (2010). Probabilistic, positional averaging predicts object-level crowding effects with letter-like stimuli. J. Vis. *10*, 14. https://doi.org/10.1167/10.10.14.
47. Levi, D.M., and Carney, T. (2009). Crowding in Peripheral Vision: Why Bigger Is Better. Curr. Biol. *19*, 1988–1993. https://doi.org/10.1016/j.cub.2009.09.056.
48. Livne, T., and Sagi, D. (2007). Configuration influence on crowding. J. Vis. *7*, 4.1–412. https://doi.org/10.1167/7.2.4.
49. Herzog, M.H., and Fahle, M. (2002). Effects of grouping in contextual modulation. Nature *415*, 433–436. https://doi.org/10.1038/415433a.
50. Saarela, T.P., Sayim, B., Westheimer, G., and Herzog, M.H. (2009). Global stimulus configuration modulates crowding. J. Vis. *9*, 5.1–511. https://doi.org/10.1167/9.2.5.
51. Kooi, F.L., Toet, A., Tripathy, S.P., and Levi, D.M. (1994). The effect of similarity and duration on spatial interaction in peripheral vision. Spat. Vis. *8*, 255–279. https://doi.org/10.1163/156856894X00350.
52. Sayim, B., Westheimer, G., and Herzog, M.H. (2008). Contrast polarity, chromaticity, and stereoscopic depth modulate contextual interactions in vernier acuity. J. Vis. *8*, 12.1–12.9. https://doi.org/10.1167/8.8.12.
53. Herzog, M.H., Sayim, B., Chicherov, V., and Manassi, M. (2015). Crowding, grouping, and object recognition: A matter of appearance. J. Vis. *15*, 5. https://doi.org/10.1167/15.6.5.
54. Song, H., Chui, T.Y.P., Zhong, Z., Elsner, A.E., and Burns, S.A. (2011). Variation of Cone Photoreceptor Packing Density with Retinal Eccentricity and Age. Invest. Ophthalmol. Vis. Sci. *52*, 7376–7384. https://doi.org/10.1167/iovs.11-7199.
55. Domdei, N., Reiniger, J.L., Holz, F.G., and Harmening, W.M. (2021). The Relationship Between Visual Sensitivity and Eccentricity, Cone Density and Outer Segment Length in the Human Foveola. Invest. Ophthalmol. Vis. Sci. *62*, 31. https://doi.org/10.1167/iovs.62.9.31.
56. Poletti, M., Listorti, C., and Rucci, M. (2013). Microscopic Eye Movements Compensate for Nonhomogeneous Vision within the Fovea. Curr. Biol. *23*, 1691–1695. https://doi.org/10.1016/j.cub.2013.07.007.
57. Intoy, J., Mostofi, N., and Rucci, M. (2021). Fast and nonuniform dynamics of perisaccadic vision in the central fovea. Proc. Natl. Acad. Sci. USA *118*, e2101259118. https://doi.org/10.1073/pnas.2101259118.
58. Pelli, D.G. (2008). Crowding: A cortical constraint on object recognition. Curr. Opin. Neurobiol. *18*, 445–451. https://doi.org/10.1016/j.conb.2008.09.008.
59. Levi, D.M., Klein, S.A., and Aitsebaomo, A.P. (1985). Vernier acuity, crowding and cortical magnification. Vis. Res. *25*, 963–977. https://doi.org/10.1016/0042-6989(85)90207-X.
60. Intoy, J., and Rucci, M. (2020). Finely tuned eye movements enhance visual acuity. Nat. Commun. *11*, 795. https://doi.org/10.1038/s41467-020-14616-2.
61. Clark, A.M., Intoy, J., Rucci, M., and Poletti, M. (2022). Eye drift during fixation predicts visual acuity. Proc. Natl. Acad. Sci. USA *119*, e2200256119. https://doi.org/10.1073/pnas.2200256119.
62. Rucci, M., Iovin, R., Poletti, M., and Santini, F. (2007). Miniature eye movements enhance fine spatial detail. Nature *447*, 851–854. https://doi.org/10.1038/nature05866.
63. Rucci, M., and Victor, J.D. (2015). The unsteady eye: An information-processing stage, not a bug. Trends Neurosci. *20*, 1–12.
64. Ko, H.-K., Poletti, M., and Rucci, M. (2010). Microsaccades precisely relocate gaze in a high visual acuity task. Nat. Neurosci. *13*, 1549–1553. https://doi.org/10.1038/nn.2663.
65. Witten, J.L., Lukyanova, V., and Harmening, W.M. (2024). Sub-cone visual resolution by active, adaptive sampling in the human foveola. eLife *13*, RP98648. https://doi.org/10.7554/eLife.98648.
66. Ratnam, K., Domdei, N., Harmening, W.M., and Roorda, A. (2017). Benefits of retinal image motion at the limits of spatial vision. J. Vis. *17*, 30. https://doi.org/10.1167/17.1.30.
67. Steinman, R.M., and Collewijn, H. (1980). Binocular retinal image motion during active head rotation. Vis. Res. *20*, 415–429. https://doi.org/10.1016/0042-6989(80)90032-2.
68. Cherici, C., Kuang, X., Poletti, M., and Rucci, M. (2012). Precision of sustained fixation in trained and untrained observers. J. Vis. *12*, 31. https://doi.org/10.1167/12.6.31.
69. Yoon, G.-Y., and Williams, D.R. (2002). Visual performance after correcting the monochromatic and chromatic aberrations of the eye. J. Opt. Soc. Am. A Opt. Image Sci. Vis. *19*, 266–275. https://doi.org/10.1364/JOSAA.19.000266.
70. Marcos, S., Sawides, L., Gambra, E., and Dorronsoro, C. (2008). Influence of adaptive-optics ocular aberration correction on visual acuity at different luminances and contrast polarities. J. Vis. *8*, 1.1–112. https://doi.org/10.1167/8.13.1.
71. Moon, B., Poletti, M., Roorda, A., Tiruveedhula, P., Liu, S.H., Linebach, G., Rucci, M., and Rolland, J.P. (2024). Alignment, calibration, and validation of an adaptive optics scanning laser ophthalmoscope for high-resolution human foveal imaging. Appl. Opt. *63*, 730–742. https://doi.org/10.1364/AO.504283.
72. Roorda, A., Romero-Borja, F., III, Donnelly, W., Queener, H., Hebert, T.J., and Campbell, M.C.W. (2002). Adaptive optics scanning laser ophthalmoscopy. Opt. Express *10*, 405–412. https://doi.org/10.1364/OE.10.000405.
73. Dubra, A., and Sulai, Y. (2011). Reflective afocal broadband adaptive optics scanning ophthalmoscope. Biomed. Opt. Express *2*, 1757–1768. https://doi.org/10.1364/BOE.2.001757.
74. Yang, Q., Arathorn, D.W., Tiruveedhula, P., Vogel, C.R., and Roorda, A. (2010). Design of an integrated hardware interface for AOSLO image capture and cone-targeted stimulus delivery. Opt. Express *18*, 17841–17858. https://doi.org/10.1364/OE.18.017841.
75. Arathorn, D.W., Yang, Q., Vogel, C.R., Zhang, Y., Tiruveedhula, P., and Roorda, A. (2007). Retinally stabilized cone-targeted stimulus delivery. Opt. Express *15*, 13731–13744. https://doi.org/10.1364/OE.15.013731.
76. Stevenson, S.B., and Roorda, A. (2005). Correcting for miniature eye movements in high resolution scanning laser ophthalmoscopy. Proc. SPIE *5688*, 0277–0786X. https://doi.org/10.1117/12.591190.
77. Zhang, M., Gofas-Salas, E., Leonard, B.T., Rui, Y., Snyder, V.C., Reecher, H.M., Mecê, P., and Rossi, E.A. (2021). Strip-based digital image registration for distortion minimization and robust eye motion measurement from scanned ophthalmic imaging systems. Biomed. Opt. Express *12*, 2353–2372. https://doi.org/10.1364/BOE.418070.
78. Kilpeläinen, M., Putnam, N.M., Ratnam, K., and Roorda, A. (2021). The retinal and perceived locus of fixation in the human visual system. J. Vis. *21*, 9. https://doi.org/10.1167/jov.21.11.9.
79. Prahalad, K.S., and Coates, D.R. (2022). Microsaccadic correlates of covert attention and crowding. J. Vis. *22*, 15. https://doi.org/10.1167/jov.22.10.15.
80. Kuang, X., Poletti, M., Victor, J.D., and Rucci, M. (2012). Temporal Encoding of Spatial Information during Active Visual Fixation. Curr. Biol. *22*, 510–514. https://doi.org/10.1016/j.cub.2012.01.050.

81. Tripathy, S.P., and Cavanagh, P. (2002). The extent of crowding in peripheral vision does not scale with target size. Vis. Res. *42*, 2357–2369. https://doi.org/10.1016/S0042-6989(02)00197-9.

82. Tripathy, S.P., Cavanagh, P., and Bedell, H.E. (2014). Large crowding zones in peripheral vision for briefly presented stimuli. J. Vis. *14*, 11. https://doi.org/10.1167/14.6.11.

83. Reiniger, J.L., Domdei, N., Holz, F.G., and Harmening, W.M. (2021). Human gaze is systematically offset from the center of cone topography. Curr. Biol. *31*, 4188–4193.e3. https://doi.org/10.1016/j.cub.2021.07.005.

84. Watson, A.B. (2014). A formula for human retinal ganglion cell receptive field density as a function of visual field location. J. Vis. *14*, 15. https://doi.org/10.1167/14.7.15.

85. Strasburger, H. (2022). On the cortical mapping function – Visual space, cortical space, and crowding. Vis. Res. *194*, 107972. https://doi.org/10.1016/j.visres.2021.107972.

86. Schira, M.M., Tyler, C.W., Breakspear, M., and Spehar, B. (2009). The Foveal Confluence in Human Visual Cortex. J. Neurosci. *29*, 9050–9058. https://doi.org/10.1523/JNEUROSCI.1760-09.2009.

87. He, D., Wang, Y., and Fang, F. (2019). The Critical Role of V2 Population Receptive Fields in Visual Orientation Crowding. Curr. Biol. *29*, 2229–2236.e3. https://doi.org/10.1016/j.cub.2019.05.068.

88. Intoy, J., Li, Y.H., Bowers, N.R., Victor, J.D., Poletti, M., and Rucci, M. (2024). Consequences of eye movements for spatial selectivity. Curr. Biol. *34*, 3265–3272.e4. https://doi.org/10.1016/j.cub.2024.06.016.

89. Anderson, A.G., Olshausen, B.A., Ratnam, K., and Roorda, A. (2016). A neural model of high-acuity vision in the presence of fixational eye movements. In Asilomar Conf. Signals Syst. Comput, pp. 588–592. https://doi.org/10.1109/ACSSC.2016.7869110.

90. Danilova, M.V., and Bondarko, V.M. (2007). Foveal contour interactions and crowding effects at the resolution limit of the visual system. J. Vis. *7*, 25.1–18. https://doi.org/10.1167/7.2.25.

91. Lev, M., Yehezkel, O., and Polat, U. (2014). Uncovering foveal crowding? Sci. Rep. *4*, 4067. https://doi.org/10.1038/srep04067.

92. Tuten, W.S., Cooper, R.F., Tiruveedhula, P., Dubra, A., Roorda, A., Cottaris, N.P., Brainard, D.H., and Morgan, J.I.W. (2018). Spatial summation in the human fovea: Do normal optical aberrations and fixational eye movements have an effect? J. Vis. *18*, 6. https://doi.org/10.1167/18.8.6.

93. Qian, M., Wang, J., Gao, Y., Chen, M., Liu, Y., Zhou, D., Lu, H.D., Zhang, X., Hu, J.M., and Roe, A.W. (2024). Multiple loci for foveolar vision in macaque monkey visual cortex. Nat. Neurosci. *28*, 137–149. https://doi.org/10.1038/s41593-024-01810-4.

94. Fischer, B. (1973). Overlap of receptive field centers and representation of the visual field in the cat's optic tract. Vis. Res. *13*, 2113–2120. https://doi.org/10.1016/0042-6989(73)90188-0.

95. Azzopardi, P., and Cowey, A. (1993). Preferential representation of the fovea in the primary visual cortex. Nature *361*, 719–721. https://doi.org/10.1038/361719a0.

96. Azzopardi, P., and Cowey, A. (1996a). Models of ganglion cell topography in the retina of macaque monkeys and their application to sensory cortical scaling. Neuroscience *72*, 617–625. https://doi.org/10.1016/0306-4522(95)00588-9.

97. Azzopardi, P., and Cowey, A. (1996b). The overrepresentation of the fovea and adjacent retina in the striate cortex and dorsal lateral geniculate nucleus of the macaque monkey. Neuroscience *72*, 627–639. https://doi.org/10.1016/0306-4522(95)00589-7.

98. Adams, D.L., and Horton, J.C. (2003). A Precise Retinotopic Map of Primate Striate Cortex Generated from the Representation of Angioscotomas. J. Neurosci. *23*, 3771–3789. https://doi.org/10.1523/JNEUROSCI.23-09-03771.2003.

99. Petrov, Y., Popple, A.V., and McKee, S.P. (2007). Crowding and surround suppression: Not to be confused. J. Vis. *7*, 12.1–12.9. https://doi.org/10.1167/7.2.12.

100. Chastain, G. (1982). Confusability and interference between members of parafoveal letter pairs. Percept. Psychophys. *32*, 576–580. https://doi.org/10.3758/BF03204213.

101. Strasburger, H., and Malania, M. (2013). Source confusion is a major cause of crowding. J. Vis. *13*, 24. https://doi.org/10.1167/13.1.24.

102. Poletti, M., Listorti, C., and Rucci, M. (2010). Stability of the Visual World during Eye Drift. J. Neurosci. *30*, 11143–11150. https://doi.org/10.1523/JNEUROSCI.1925-10.2010.

103. Korte, W. (1923). Über die Gestaltauffassung im indirekten Sehen. Z. Psychol. *93*, 17–82.

104. Banks, W.P., Larson, D.W., and Prinzmetal, W. (1979). Asymmetry of visual interference. Percept. Psychophys. *25*, 447–456. https://doi.org/10.3758/BF03213822.

105. Herzog, M.H., and Manassi, M. (2015). Uncorking the bottleneck of crowding: A fresh look at object recognition. Curr. Opin. Behav. Sci. *1*, 86–93. https://doi.org/10.1016/j.cobeha.2014.10.006.

106. Cicchini, G.M., D'Errico, G., and Burr, D.C. (2022). Crowding results from optimal integration of visual targets with contextual information. Nat. Commun. *13*, 5741. https://doi.org/10.1038/s41467-022-33508-1.

107. Manassi, M., Sayim, B., and Herzog, M.H. (2012). Grouping, pooling, and when bigger is better in visual crowding. J. Vis. *12*, 13. https://doi.org/10.1167/12.10.13.

108. Manassi, M., Sayim, B., and Herzog, M.H. (2013). When crowding of crowding leads to uncrowding. J. Vis. *13*, 10. https://doi.org/10.1167/13.13.10.

109. Cooper, R.F., Wilk, M.A., Tarima, S., and Carroll, J. (2016). Evaluating Descriptive Metrics of the Human Cone Mosaic. Invest. Ophthalmol. Vis. Sci. *57*, 2992–3001. https://doi.org/10.1167/iovs.16-19072.

110. Schütt, H.H., Harmeling, S., Macke, J.H., and Wichmann, F.A. (2016). Painfree and accurate Bayesian estimation of psychometric functions for (potentially) overdispersed data. Vis. Res. *122*, 105–123. https://doi.org/10.1016/j.visres.2016.02.002.

111. Tuten, W.S., Harmening, W.M., Sabesan, R., Roorda, A., and Sincich, L.C. (2017). Spatiochromatic Interactions between Individual Cone Photoreceptors in the Human Retina. J. Neurosci. *37*, 9498–9509. https://doi.org/10.1523/JNEUROSCI.0529-17.2017.

112. Greene, M.J., Pandiyan, V.P., Sabesan, R., and Tuten, W.S. (2025). Local variations in L/M ratio influence the detection and color naming of small spots. J. Vis. *25*, 13. https://doi.org/10.1167/jov.25.12.13.

113. Watson, A.B., and Pelli, D.G. (1979). The QUEST staircase procedure. Appl. Vis. Assoc. Newsl. *14*, 6–7.

114. Hamwood, J., Alonso-Caneiro, D., Sampson, D.M., Collins, M.J., and Chen, F.K. (2019). Automatic Detection of Cone Photoreceptors With Fully Convolutional Networks. Transl. Vis. Sci. Technol. *8*, 10. https://doi.org/10.1167/tvst.8.6.10.

115. Cunefare, D., Fang, L., Cooper, R.F., Dubra, A., Carroll, J., and Farsiu, S. (2017). Open source software for automatic detection of cone photoreceptors in adaptive optics ophthalmoscopy using convolutional neural networks. Sci. Rep. *7*, 6620. https://doi.org/10.1038/s41598-017-07103-0.

116. Gutnikov, A., Hähn-Schumacher, P., Ameln, J., Zadeh, S.G., Schultz, T., and Harmening, W. (2025). Neural network assisted annotation and analysis tool to study in-vivo foveolar cone photoreceptor topography. Sci. Rep. *15*, 23858. https://doi.org/10.1038/s41598-025-08028-9.

STAR★METHODS

KEY RESOURCES TABLE

REAGENT or RESOURCE	SOURCE	IDENTIFIER
Deposited data		
Original psychophysics data	This paper	https://osf.io/yugdj
Software and algorithms		
Custom MATLAB code for data analysis and figure generation	This paper	https://osf.io/yugdj
MATLAB (R2022b)	MathWorks	https://www.mathworks.com; RRID: SCR_001622
BayesFactor MATLAB toolbox	Lab of Cognitive Neuroscience, K- Lab	https://github.com/klabhub/bayesFactor
Metricks[109]	AOIP Lab	https://github.com/AOIPLab/Metricks
psignifit 4[110]	Wichmann Lab	https://github.com/wichmannlab/psignifit

i-

EXPERIMENTAL MODEL AND STUDY PARTICIPANT DETAILS

Observers

Eight experienced observers (5 males and 3 females; age range: 25-31 years) with normally sighted vision and refractive errors less than 4 diopters in magnitude participated in the study. Four of the eight subjects were authors of the study. The experiment was performed monocularly and the non-tested eye was occluded with an eye patch. Visual acuity was confirmed to be 20/20 or better for all subjects, with refractive errors less than 3.5 diopters and astigmatism less than -1.00 diopters in the tested eye. Prior to retinal imaging, dilation drops phenylepherine (2.5%) and tropicamide (1%) were instilled into the test eye at least fifteen minutes prior to the start of the imaging session. The experimental protocol was approved by the University of Rochester's Research subjects review board (RSRB). Written informed consent was obtained from each participant after explaining the study procedures and reviewing the consent form.

Apparatus

A custom built Adaptive Optics Scanning Light Opthalmoscope (AOSLO)(described elsewhere[71]) was used to image at high-resolution subject's retinae (diffraction limited resolution of 0.40 arcmin for 680 nm wavelength). These recordings achieve cellular level resolution necessary for precise stimulus presentation at targeted retinal locations with diffraction-limited image quality.[74,75] Additionally, this setup allowed for extraction of high resolution eye movement signals from the recorded retinal videos.[76,77] The imaging and stimulus delivery channel has a central wavelength of 680 nm and a bandwidth of 22 nm (full width at half maximum). The stimulus was generated by modulating the red light using an acousto-optic modulator (TEM-210-50-10-680-2FP-SM, Brimrose Corp., Sparks Glencoe, MD). A separate 940 nm channel was used to measure optical aberrations, which were corrected in a closed-loop system by dynamically adjusting the shape of a deformable mirror (DM97-08, ALPAO, Montbonnot, France). The imaging field of view was set to 60 x 60 arcminutes. The AOSLO frame rate is 30 Hz and the resolution is 512 x 512 pixels, with each pixel subtending $\sim$ 0.12 arcminutes.

Stimuli were presented in reverse contrast using a 680 nm raster in our AOSLO system. While this wavelength is close to the peak sensitivity of L-cones, both L- and M-cones are expected to contribute comparably under these conditions. Although L-cones are $\approx$ 20 $\times$ more sensitive than M-cones at 680 nm, the raster background induces adaptation that effectively equalizes their sensitivities, consistent with single-cone sensitivity measurements.[111,112] These findings, therefore, suggest that our stimulation was not biased toward a single cone class.

METHOD DETAILS

Imaging protocol

Once pupil dilation was achieved (pupil diameter $\geq$ 7 mm), subjects were positioned in front of the AOSLO system using a custom bite bar setup attached to a three-axis translation stage (see Figure 1A). Initial alignment was performed using the 940 nm channel, with the 680 nm channel blocked. After initiating the closed-loop adaptive optics correction and ensuring it was stable, subjects were

nformed, and the 680 nm channel was set to its maximum power and unblocked. During the experiments, we imaged approximately ~ 60 arcminutes of the central retina in the right eye of each participant using the visible red light channel of the AOSLO.

Stimulus

The stimulus consisted of digits 3,5,6 and 9 from a slightly modified version of the Pelli number font[9] which allows for testing smaller spacing between the target and flanker compared to traditional optotypes, making it an ideal candidate for testing visual crowding at the fovea, where the critical spacing is much smaller than in the periphery.[16] Each trigram, consisting of the target and two flankers, was chosen such that each element was unique, thereby avoiding repetition, which would otherwise reduce the influence of the flankers and make it difficult to compare between trials. The stimulus was presented on the imaging raster at maximum negative contrast (see example in Figure 1B). Flankers appeared along the radial axis (horizontally) at fixed target-flanker distances. We chose to avoid flankers along the vertical or tangential axis for two reasons: (1) flankers along the radial or horizontal (in the current experiment) axis tend have an increased interference with target recognition when compared to tangential or vertical flankers, this is referred to radial-tangential anisotropy[3]; (2) the pelli font is vertically elongated; therefore, having flankers along the vertical axis results in a larger stimulus array. This affects the online tracking modality because a larger part of the retina falls under the stimulus and is not imaged.

We ensured that the residual diffraction after correction did not result in overlap due to blur at the closest spacing tested. To this end, we calculated the point spread function for the diffraction limited condition (Pupil size: 7.2 mm; wavelength: 680 nm and focal length: 16.67 mm) and convolved with the crowded stimulus at the smallest spacing, where we observed no overlap between the target and the flanker, as shown in Figure S1. This validates that the change in performance at the closest spacing is driven by crowding from the flankers, rather than spatial overlap from blur.

PRL determination and high-resolution imaging

The preferred retinal locus of fixation (PRL) was determined for each individual during a separate experimental session. Subjects fixated on a maltese cross (5 x 5 arcminutes) that randomly shifted positions every 2 to 6 seconds within a 15 x 15 arcminute region of the raster whilst simultaneously recording a 30 second retinal video, similar to the method followed previously.[78] The raw retinal videos were analyzed offline using REMMIDE,[77] which uses a strip based cross correlation technique (described in[76]) to generate stabilized retinal videos and images accounting for retinal motion. We excluded 20 frames (~ 666 ms) following each positional change of the maltese cross to account for microsaccades that reposition the PRL onto the maltese cross. The stimulus location on the remaining frames was overlaid onto the stabilized retinal image and the median stimulus location was used to determine the PRL location.

A high-resolution image of each participant was obtained in a separate experimental session. Subjects fixated on a black square (4.69 × 4.69 arcminutes flickering on and off at 3 Hz with a duty cycle of 0.5) presented at a fixed location at the center of the imaging raster. For each participant, we recorded 6-12 videos, with each one being 10 seconds long. These recordings were processed using REMMIDE[77] to generate a frame average with minimal distortion, and the one that provided the best image quality was selected as the high-resolution image for the subject. The PRL coordinates were then mapped onto the high-resolution image.

Experiment 1: Stabilized condition at PRL

A QUEST procedure[113] with 3 interleaved staircases converging at 62.5% was used to determine the size threshold for each individual when stimuli were viewed at the PRL in isolation under retinal stabilization. We excluded data from staircases in which the stimulus size was at ceiling for more than 5 consecutive trials. This could occur if the online stabilization algorithm failed, resulting in an altered stimulus appearance. The threshold size was chosen based on convergence levels from at least 2 staircases. The stimulus size in the main experiment was set to be three times the threshold size obtained with the QUEST procedure.[3,79]

Experiment 1 was performed under retinal stabilization, where the stimulus was presented either in isolation or surrounded by flankers to the left and right of the stimulus for 15 frames or ~ 500 ms. Importantly, the stabilized presentation did not induce perceptual fading: stimuli were brief (500 ms), flashed (strong onset/offset transient), and shown at maximum negative contrast; moreover, performance in the unflanked condition was at or near ceiling, confirming preserved visibility. When flankers were present, they were positioned at one of five different spacings, with spacings defined as the edge-to-edge distance between the target and each flanker. The spacings ranged between 0.12 to 3.5 arcminutes, with a mean step size of 0.34 arcminutes. Performance was also tested in the unflanked condition. Each subject completed ~ 10-15 blocks with each block consisting of 60 trials, with 10 repetitions at each flanker spacing plus 10 interleaved unflanked trials. The sequence of flanker spacings was randomized within each block. An example frame from a retinal video recording is shown in Figure 1C. A 1 second video (30 frames) was captured for each trial with the stimulus presented after a blank interval of 10 frames or 330 ms. Observers used a joypad to initiate each trial and responded at the end of the trial upon hearing a beep, with unlimited time to respond. After each trial, observers manually started the subsequent trial at their own pace (self-paced).

Experiment 2: Stabilized condition 15′ away from PRL

Experiment 2 followed the same procedure as Experiment 1 but targeted a location 15′ from the PRL. Thresholds were re-estimated and stimuli scaled 3 × accordingly.

Experiment 3: Unstabilized condition

The stimulus was presented in the center of the imaging raster and remained at the center throughout the entire presentation interval. As in experiments 1 and 2, the size of the stimulus was scaled based on a QUEST procedure performed in the unstablized condition prior to the main experiment. As visual acuity thresholds are generally lower (*i.e.*, better acuity) in the unstablized vs stabilized condition,[60,61,66] we ensured that stimulus sizes were scaled to account for the differences in visual acuity between the two conditions. Stimuli were rendered at a fixed screen location (center of raster), resulting in retinal motion due to ocular drift. A separate QUEST procedure determined acuity thresholds under unstabilized viewing.

Online retinal stabilization procedure

Prior to the start of experiment 1, subjects were instructed to fixate on a marker in the center of the imaging raster. The experimenter manually captured a single video frame, which provided robust real-time (online) tracking. This frame was registered with the high-resolution retinal image containing the PRL coordinates, and the pixel coordinates corresponding to the PRL were mapped onto the single frame. This image was obtained in a prior assessment of the PRL (see section PRL Determination). To ensure robust registration, the experimenter manually checked for shifts in landmarks between the two images and confirmed that the PRL coordinates were close to the center of the frame. This ensured that, during the experiment, the stimulus was maintained at the PRL coordinates, close to the center, and that it remained centered in the raster and well stabilized. Once registration was confirmed, the marked single frame served as the global reference for the session. Whenever stimulus rendering or online stabilization was found to be inadequate, *i.e.*, when the retinal landmarks abruptly jumped on the online registration panel or when the stimulus was not completely rendered, this step was repeated to maintain accuracy. The single frame with the PRL coordinates was reloaded into the imaging software (ICANDI;[74,75]) to ensure that the stimulus in the experiment would be presented at the PRL.

In experiment 2, observers were instructed to fixate on a marker positioned approximately 15′ to the left of the center of the raster. A single frame providing robust real-time tracking was captured and, as in Experiment 1, registered with the global reference. The pixel coordinates corresponding to a location 15′ to the right of the PRL were mapped onto this reference frame, aligning the new fixation position. The single frame containing pixel coordinates 15′ from the PRL was subsequently reloaded into ICANDI. In addition to presenting the stimulus at the target location, a secondary stimulus (a fixation cross) was presented near the PRL and was not stabilized on the retina. This secondary stimulus (fixation cross) was included to assist subjects in maintaining fixation during the trial.

QUANTIFICATION AND STATISTICAL ANALYSIS

Offline video processing

The delivery of the stimulus at the intended PRL location depended on the robustness of the online tracking modality. To ensure precise stimulus delivery, we processed the raw videos using the strip-based registration technique[77] and determined the stimulus location on each frame from the stabilized retinal video to quantify the accuracy of stimulus delivery. We calculated the offset of the stimulus location in each individual frame by comparing it to the average pixel position of all stimulus locations for a given subject. We excluded trials in which the stimulus offset exceeded 1 arcminute from the average stimulus location on more than 10 out of 15 frames ($\sim$ 500 ms) when the stimulus appeared (see Figure 1D). On average, each subject completed 461 $\pm$ 230 trials, approximately half of these trials (54% $\pm$ 23%) met the stimulus offset criteria and were included in the final analysis. This can occur due to poor registration between an individual frame of the video and the reference image caused by poor image quality or failed online registration in the presence of rapid gaze shifts, such as microsaccades or saccades.

Cone-tagging procedure

The cropped high-resolution retinal images generated by the strip based registration software[77] (see section "PRL determination and high-resolution imaging") was used to identify and mark individual cones with a semi-automated procedure that utilizes a fully convolutional network[114] trained using several manually tagged high-resolution images of the retina (see Reiniger et al.[83] and Cunefare et al.[115]). This analysis was performed using ConeMapper,[116] an open-source tool designed for cone detection and analysis. The tagged cone locations were then checked by a single trained experimenter and manual correction was applied wherever necessary.

Determining the cones stimulated by the stimulus array

We determined the cones stimulated by the visual input based on the stimulus position on the high-resolution retinal image acquired earlier (see section "PRL determination and high-resolution imaging"). Each trial in the experiment provided 10-15 samples of the stimulus location, which were used to position the stimulus, at the tested size and threshold spacing for each subject, on the high-resolution retinal image. We then determined which cones were stimulated by the stimulus in each frame, and identified the set of cones stimulated during the 500 ms presentation. The probability of each cone being within the region of interest being stimulated during the 500 ms presentation interval (approximately 15 frames) was also calculated.

Shared cone stimulation

To determine the probability that a single cone was stimulated by both the target and either of the flankers within a single trial, we identified the unique set of cones stimulated by both the target and the flankers and normalized this by the total number of cones falling under the target in each trial. To ensure consistency across subjects, we included only the subset of trials with all 15 frames

valid, corresponding to the entire duration of the stimulus presentation (500 ms). Finally, we calculated the average probability that a single cone was stimulated by both the target and either one of the flankers across trials.

Cone spacing calculation

Each participant's high-resolution retinal image was used to analyze cone spacing in the region of interest (ROI). The stimulus, consisting of the target and flankers—at the tested stimulus size and at the subject's threshold spacing, was placed at the foveal cone mosaic location corresponding to the median stimulus location across trials in a given condition. Cone locations encompassed by the whole stimulus array (red and green circles in Figure 2B) were then identified for subsequent analysis. Cone spacing was computed by averaging the Euclidean distances between each cone and its neighboring cones in a triangulated mesh. This spacing was calculated for the subset of cones within the ROI, defined as the largest area encompassed by the stimulus (target and flankers) across all trials, using Metricks.[109] Within the foveola, it is a reasonable assumption that center-to-center cone spacing closely matches cone diameter, given that cones in this region are tightly packed with minimal inter-cone spacing. The average cone diameter in this area was then used for subsequent analysis. Thus, the cone diameter estimate within the ROI was used to define the target-flanker spacings as multiples of cone diameter.

Estimation of critical spacings

Critical spacing was defined as the distance between the target and flanker at which desired performance level is achieved. Critical spacing thresholds were estimated by fitting the data (performance measures vs. flanker spacing) using a Weibull psychometric function implemented in psignifit.[110] Based on the psychometric fit, the spacing threshold was defined as the spacing resulting in a 25% drop from the asymptote.[79] We reported critical spacing thresholds as edge-to-edge separations. We choose to report edge-to-edge spacing instead of center-to-center spacing because edge-to-edge is considered a more appropriate measure for foveal crowding.[11,16] The critical spacing corresponds to the spatial extent over which crowding impacts performance, thus smaller critical spacing's indicate less interference from crowding.

Defining critical spacing in cortical units

To assess whether cortical scaling could account for eccentricity effects, critical spacing thresholds were converted into millimeters of cortical distance using the formulation described by Strasburger.[85] Specifically, cortical critical spacing (κ) was computed as

$$\kappa = M_0 \cdot E_2 \cdot \ln\left(1 + \frac{\delta_0}{E_2} \cdot \frac{1+E/\widehat{E}_2}{1+E/E_2}\right) \quad \text{(Equation 1)}$$

where M_0 is the foveal cortical magnification factor (mm/deg), E_2 is the eccentricity constant at which magnification falls to half its foveal value (deg), δ_0 is the foveal critical spacing (deg), E is the retinal eccentricity (deg), and $\widehat{E}_2$ is the psychophysical eccentricity constant at which the threshold doubles relative to the fovea.

High-resolution fMRI measurements from Schira et al.[86] were used to set the cortical magnification parameters. For V1, we used $M_0 = 28$ mm/deg and $E_2 = 0.312^\circ$. For V2, we used $M_0 = 45$ mm/deg and $E_2 = 0.147^\circ$. Following the approach of Strasburger,[85] $\widehat{E}_2$ was estimated directly from our behavioral data by fitting linear regressions to the inverse magnification function and determining the eccentricity at which the baseline value doubled. This yielded $\widehat{E}_2 = 0.312^\circ$ for V1 and $\widehat{E}_2 = 0.147^\circ$ for V2.

Statistical analysis

Analysis of variance

Statistical comparisons were conducted using two-way repeated-measures analyses of variance (RANOVA in MATLAB) with subject and condition as within-subject factors. For all repeated-measures factors, Mauchly's test was used to assess sphericity. Greenhouse–Geisser–corrected p-values p_{GG} are reported where applicable. For two-level within-subject factors, sphericity corrections were unnecessary p_{GG} =p. Post hoc comparisons were performed using Tukey–Kramer tests in MATLAB to identify pairwise differences among conditions.

Pairwise comparisons

Planned pairwise comparisons between experimental conditions were conducted using paired two-tailed t -tests. To complement classical inference, Bayes factors (BF_{10}) were computed using the BayesFactor MATLAB toolbox (GitHub repository), providing a continuous measure of evidence for the alternative versus null hypothesis. Cohen's d was also calculated to quantify the magnitude of the observed effects.

Reporting summary

All statistical tests were two-tailed with a significance threshold of $\alpha = 0.05$. Data are reported as mean ± SEM unless otherwise stated. Statistical analyses were performed using custom scripts in MATLAB R2022b (MathWorks, Natick, MA).

Current Biology, Volume *35*

Supplemental Information

Non-uniform signal pooling across the foveola

Krishnamachari S. Prahalad, Ashley M. Clark, Benjamin Moon, Austin Roorda, Pavan Tiruveedhula, Wolf Harmening, Aleksandr Gutnikov, Samantha K. Jenks, Sanjana Kapisthalam, Michele Rucci, Jannick P. Rolland, and Martina Poletti

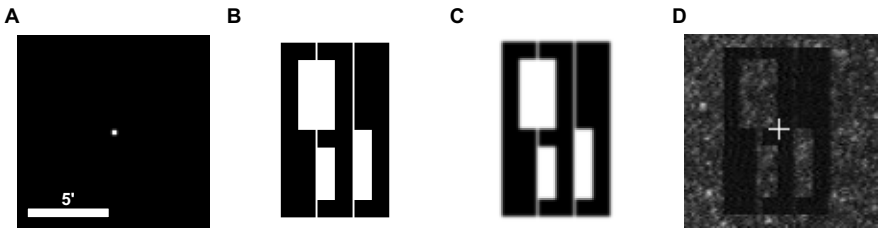

Figure S1. Stimulus configuration and retinal image fidelity, related to Figure 1B, C. To rule out the possibility that residual diffraction after correcting for ocular aberrations did not lead to an overlap of stimulus and flankers for the smallest spacing tested. We calculated the point spread function (PSF) for the diffraction limited condition **A** (wavelength: 680 nm; pupil size: 7.2 mm and focal length of 16.67 mm) and convolved it with the crowded stimulus at the smallest spacing (∼0.12 arcmin) **B**. The resulting image is shown in **C**, while **D** shows an example frame from the retinal video during the experiment from Subject S5, illustrating the appearance of the stimulus configuration over the subject's cone mosaic. Although there was a slight blur of the stimuli due to diffraction, the boundaries of the stimuli remained clearly visible, and their separation was preserved in the retinal image.

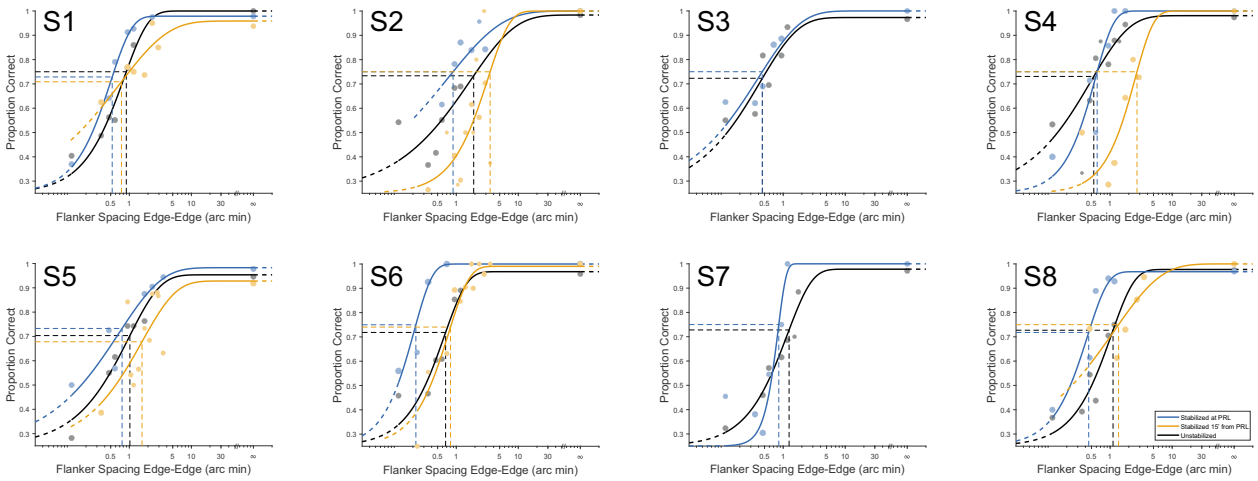

Figure S2. Individual psychometric functions for each subject, related to Figure 1E. Blue points show the stabilized condition at the PRL, orange points show the stabilized condition at 15 arcmin from the PRL, and black points show the unstabilized condition. Solid lines indicate the fitted psychometric functions, and dashed lines mark the estimated critical spacing thresholds (arcmin).

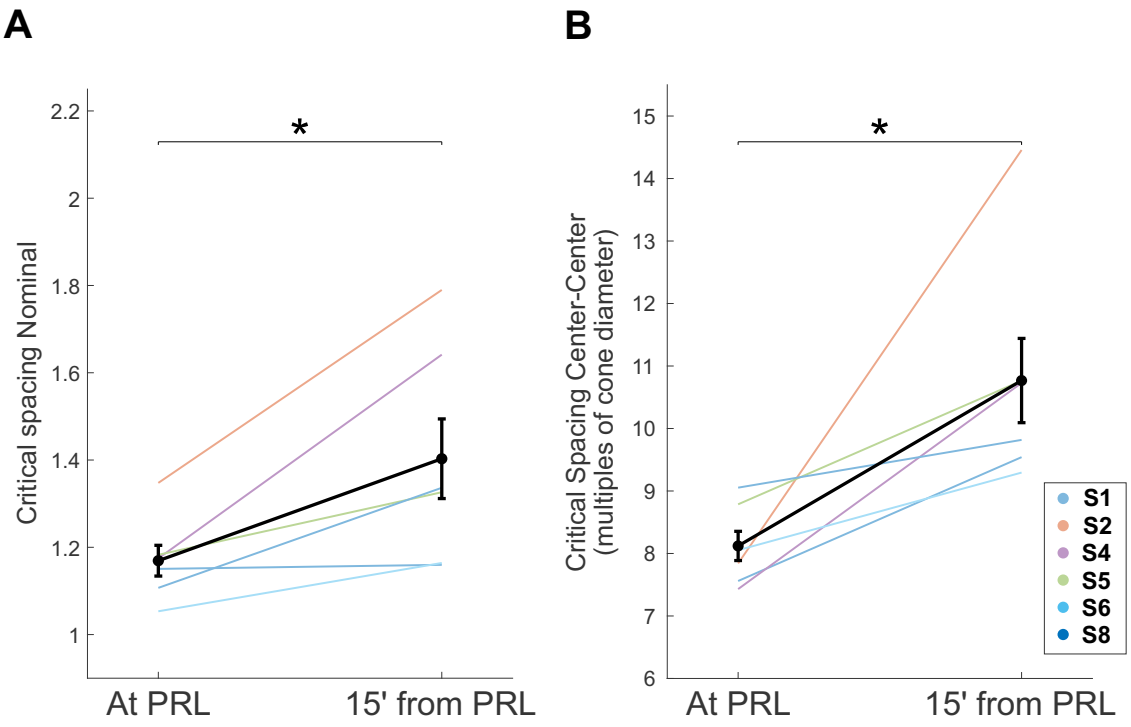

Figure S3. Alternate representations of critical spacings, related to Figure 3H. Comparison of critical spacing represented as **A** nominal spacings (center-to-center spacing / target width) and **B** center-to-center estimates represented as multiples of cone diameter between stimuli presented at the PRL and when presented 15 arcmin from the PRL. The solid lines represent the $mean \pm sem$ critical spacing measures across subjects in each condition. Critical spacing was larger for the 15 arcmin from PRL condition compared to stimuli presented at the PRL, both when represented as nominal spacing ($t(5) = 28.74$, $^{*}p = 0.03$, $BF_{10} = 3.27$, Cohen's $D = 1.00$) and as center-to-center estimates in multiples of cone diameter ($t(5) = 30.07$, $^{*}p = 0.03$, $BF_{10} = 3.16$, Cohen's $D = 1.56$).

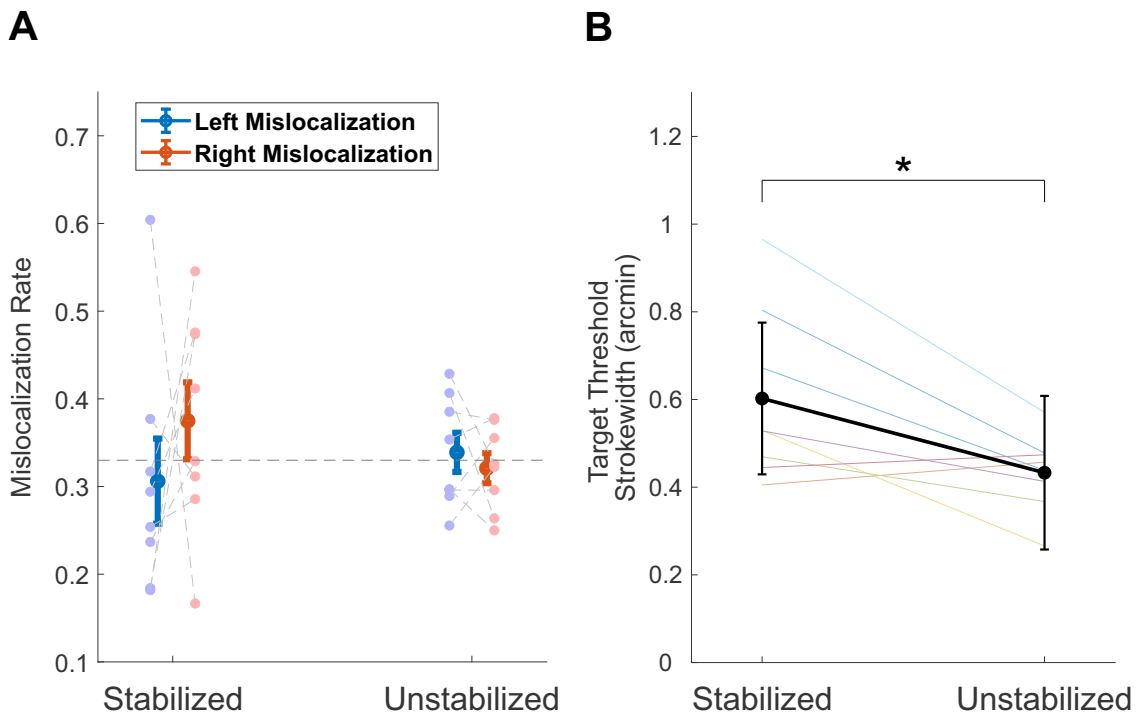

Figure S4. Mislocalization and Visual Acuity Thresholds: A comparison between stabilized stimuli at the Preferred Retinal Locus (Experiment 1) and unstabilized stimuli (Experiment 3). Related to Figures 5C and 6. A The probabilities of reporting one of the two flanker digits (inner and outer) on incorrect trials are plotted for each subject for trials where the stimulus was stabilized at the PRL and for trials where it remained at a fixed location on the raster (unstabilized condition). Error bars indicate sem. Mislocalization rates were comparable in the stabilized and unstabilized conditions (repeated measures ANOVA: $F\,(1,\,7) = 0.269$, $p = 0.62$). The probabilities of reporting the left vs. the right flanker were also comparable in both conditions (repeated measures ANOVA: $F\,(1,\,7) = 0.247$, $p = 0.634$). **B** Comparison of the threshold target stroke-width between the stabilized and unstabilized conditions. We observed an improvement in visual acuity, *i.e.*, smaller stroke-width thresholds, in the unstabilized condition ($t(5) = 2.95$, $*p = 0.02$, $BF_{10} = 3.62$, Cohen's $D = 0.99$).

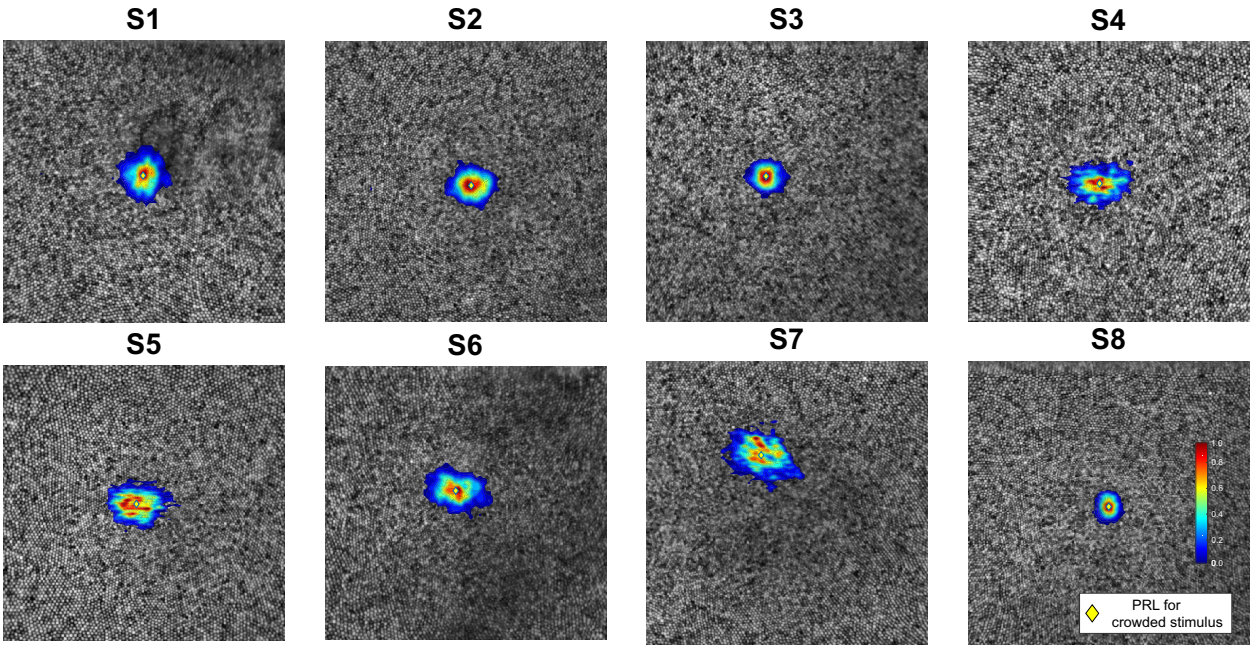

Figure S5. Stimulus landing distribution, related to Figure 6A. The stimulus distribution maps in the unstabilized viewing condition are overlaid on the retinal cone mosaic for individual subjects. The PRL is highlighted by the yellow diamond.

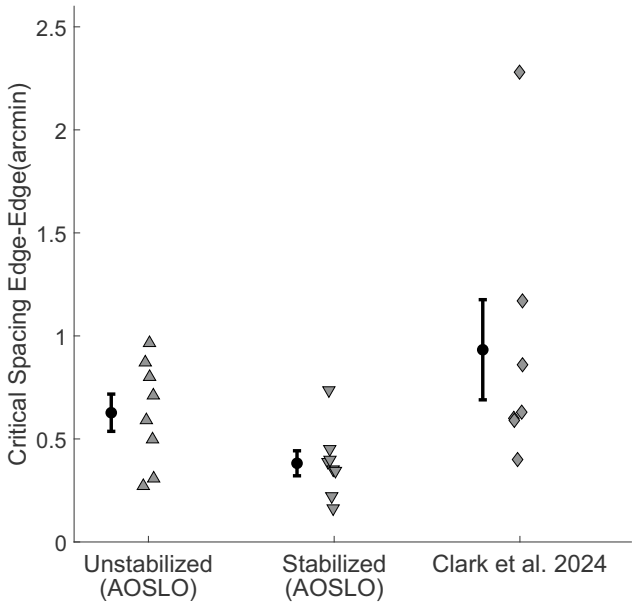

Figure S6. Comparison of edge-to-edge (E2E) critical spacing across studies examining foveal crowding with similar stimuli, related to Figure 6. Data shown are from (1) the unstabilized AOSLO condition of the current study, where stimuli were presented under diffraction limited condition but the retinal motion from fixational eye movements was not compensated; (2) the stabilized AOSLO condition of the current study, in stimuli were presented under diffraction limited viewing and were retinally stabilized; and (3) Clark et al. (2024), unstabilized viewing condition in the presence of physiological optical aberrations (Figure 7), trials with microsaccades and saccades were excluded, and gaze constrained within 30 arcminutes during stimulus presentation. Statistical comparison using Wilcoxon rank-sum tests showed no significant difference between the unstabilized AOSLO condition and Clark et al. 2024 (Wilcoxon rank–sum test, $W = 57$, $p = 0.463$). On the other hand, thresholds in the stabilized condition were significantly smaller than those from Clark et al. 2024 (Wilcoxon rank–sum test, $W = 41$, $p = 0.006$).